

BIOORTHOGONAL FLUORESCENT LABELS: A REVIEW ON COMBINED FORCES

Gergely B. Cserép, András Herner and Péter Kele*

Address: Chemical Biology Research Group, Hungarian Academy of Sciences, Research Centre for Natural Sciences, Institute of Organic Chemistry, H-1117 Magyar tudósok krt. 2, Budapest, Hungary

e-mail: kele.peter@ttk.mta.hu

Abstract

This review ventures upon to summarize the latest developments in bioorthogonal fluorescent imaging labels with a special focus on bioimaging applications. We briefly summarize the most preferred means of bioorthogonal tagging schemes for the labeling of specific biomolecular structures. The review is structured by the type of the fluorescent labels that can address the problems that most commonly compromise fluorescent imaging techniques i.e. autofluorescence of biomolecules, background fluorescence of unreacted reagents and photobleaching. Thus we present i) far-red / near-infra-red emitting dyes, ii) fluorogenic scaffolds and iii) nanoparticle based signaling platforms.

1. Introduction

In line with the growing needs of chemical biology, progress in bioorthogonal chemistry has brought great advances in bioconjugation related techniques. Since Bertozzi and Saxon has formulated the postulates for bioorthogonality in 2002 a set of bioorthogonal reactions was delineated.[1] Covalent modification of biomolecules by means of bioorthogonal reactions rely on the ready and selective (orthogonal) reactions of biocompatible, non-natural cognate functions inside living systems while they do not interfere with the multitude of endogenous groups (e.g. thiols, amines) present in biomolecules.[2,3,4,5,6,7] Most bioorthogonal tagging reactions follow a two-step manipulation scheme. First, the biomolecule of interest is modified with one of the bioorthogonal functions (chemical reporter) by means of chemical, enzymatic, metabolic incorporation or protein engineering. Then the bioorthogonalized system can be selectively targeted with a secondary reagent (marker, affinity label etc.) harboring the

complementary bioorthogonal function.[1-7] These lately developed reactions enable controlled and exquisite manipulation of biomolecules. Such manipulated systems then can be used to interrogate biological systems in order to get deeper insight into biomolecular processes. Since fluorescent microscopy techniques offer excellent temporal and spatial resolution for the monitoring of these *in vivo* processes, most bioorthogonal tagging schemes involve fluorescent modulation of the biomolecule of interest.[8]

In this review we discuss the latest developments in bioorthogonal fluorescent labeling techniques with a special focus on bioimaging applications using different fluorescent species. We briefly summarize the most preferred bioorthogonal tagging schemes together with the possible means for the bioorthogonalization of biomolecular structures. At the end we attempt to give some insights into the future challenges of the field.

2. Bioorthogonal reactions

The early 2000s resulted in the delineation of a set of reactions with the potential to be applicable in living systems. Several, related and recent reviews list all these chemistries in details.[1-7] Although wider selections of bioorthogonal reactions list more chemical transformations e.g. aldehyde/ketone-amine ligations, herein we restrict our discussion to chemistries that either use purely non-natural functions or non-natural combinations of natural functions (e.g. Cys₄-tag) to ensure selective ligation (Figure 1).

2.1. Staudinger-(Bertozzi) ligation

Triaryl-phosphanes harboring an ester function as an electrophilic trap together with organic azides are moieties that are stable in biological media and indifferent to the presence of natural functions react readily with each other resulting in the formation of a stable amide bond.[1,9,10,11] Though this transformation is quite slow (Figure 1) and some of the reagents is lost due to spontaneous oxidation of the phosphanes, it still remains popular for its full biocompatibility, selectivity and its potential to construct fluorogenic probes.

2.2. Photoclick reaction

The reaction developed by Lin *et al.* generates nitrile imine intermediates from tetrazoles following a short pulse of UV irradiation.[12,13,14,15,16] The reactive dipolar species undergo rapid cycloaddition with olefins affording fluorescent pyrazoline derivatives (Figure 1). In spite of its need for UV irradiation the inherent fluorogenicity and photo-

controllability, which enables spatial and temporal control makes this transformation quite appealing.

2.3. Azide-alkyne cycloadditions

Similarly to the Staudinger-ligation the copper catalyzed azide-alkyne 1,3-dipolar cycloaddition (CuAAC) also makes use of the small, stable, yet highly energetic azide group.[17] This highly valuable regioselective reaction between organic azides and terminal alkynes in the presence of Cu(I) catalyst gives rise to the formation of a stable, covalent 1,4-disubstituted triazole-linkage.[18,19,20] The need for copper catalyst, however, limits the *in cell* or *in vivo* applicability of this reaction, although recent developments addressed the metal-toxicity issue by applying appropriate ligand additives to mask the toxic transition metal.[21] Besides the biocompatibility concerns, copper can also affect fluorescence of certain signaling species and irreversibly quench the fluorescence of e.g. GFPs or quantum dots. An alternative approach that eliminates the need for toxic copper catalyst was introduced by Bertozzi and co-workers.[22,23] In their respective works they demonstrated that introduction of strain into the alkyne reactant efficiently promotes the reaction to proceed at room temperature without any catalyst. Leaving the copper catalyst out had some consequences though: besides losing regioselectivity, the strain promoted azide-alkyne cycloaddition (SPAAC) proceeds at slower rates than the copper catalyzed reaction. This latter issue was addressed by many laboratories by developing more reactive cyclooctynes derivatives (Figure 1).[24,25,26,27,28]

2.4. Inverse electron demand Diels-Alder reactions

A breakthrough was achieved in catalyst-free bioorthogonal ligations with the use of tetrazines and respective strained dienophiles.[22] The strain promoted inverse electron demand Diels-Alder cycloaddition (SPIEDAC) reaction between these reactants really meets the need for demanding biological applications.[29,30,31] Although the synthesis of the reagents often require laborious synthetic work, tetrazines in combination with various strained dienophiles such as norbornenes, cyclooctynes, *trans*-cyclooctenes display the fastest reaction rates, in general, of all bioorthogonal reactions (Figure 1). The reactivity of the tetrazines could be tuned either by reducing the bulk [32] or increasing the electron withdrawing nature of substituents, however, for biological applications a trade-off should be made between reactivity and stability.[29]

Finally, it should be noted that some bioorthogonal transformations are also orthogonal to each other. For example, appropriately selected reactants enable orthogonal SPAAC and

SPIEDAC ligations.[33] Other examples report on the orthogonal use of two SPIEDAC reactions where appropriately selected tetrazines and dienophiles allowed selective modulation schemes.[34]

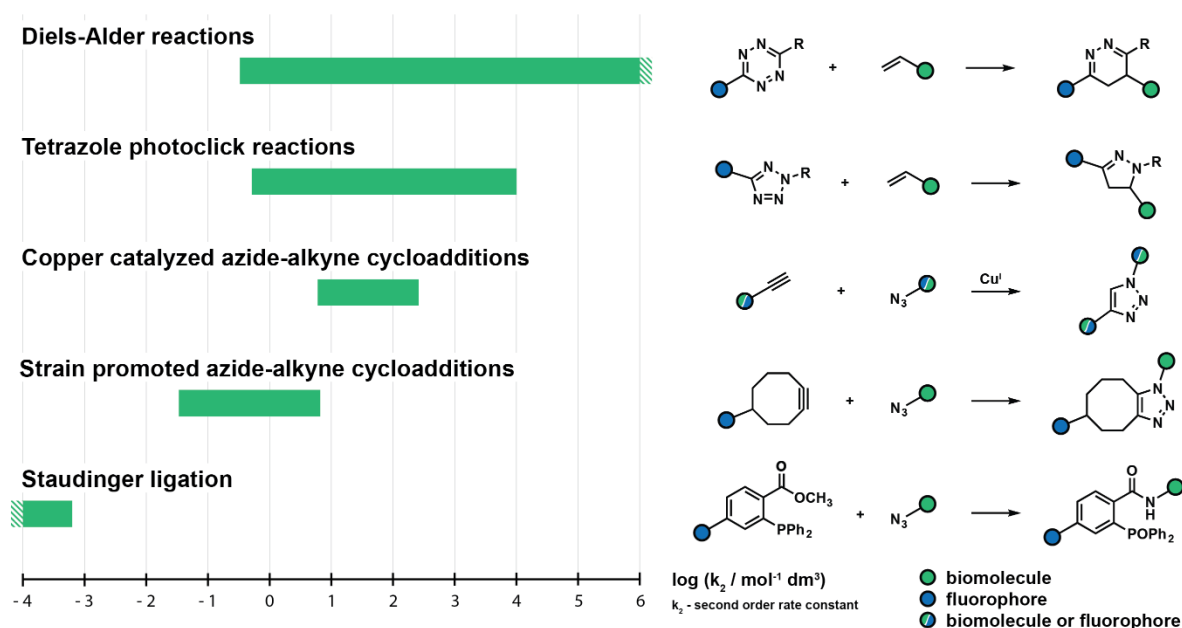


Figure 1. Comparison of reaction rates of the most used bioorthogonal reactions.

2.5. Installation of bioorthogonality

Bioorthogonal labeling strategies mostly rely on a sequential two-step modification scheme.[2-4,35] At first installation of the bioorthogonal moiety into the biomolecule of interest by means of chemical reporters is required. This step is followed by a selective modification of this chemical reporter through its bioorthogonal motif with a fluorescent marker harboring the complementary bioorthogonal function. For the incorporation of the chemical reporter tag, several options exist, however, for proteins, most methods are restricted to N- or C-terminal modifications. For instance, proteins can be manipulated selectively through their C- or N-termini using mild chemistries.[2,36,37,38,39] Other methods to affix bioorthogonal moieties onto proteins include selective derivatization through rare building blocks e.g. Cys or Tyr residues.[40,41,42,43] Installation of chemical reporter tags is also possible e.g. by means of enzymatic tagging platforms.[44] Truly site-specific decoration of the protein of interest with bioorthogonal function is enabled by means of amino acid mutagenesis using orthogonal AARS/tRNA pairs.[45,46,47]

Fewer methods exist for the bioorthogonalization of non-proteinaceous species (lipids, sugars, nucleic acids).[48] Examples for the use of direct chemical modification or mutant enzymes of such scaffolds exist, however mostly limited to *in vitro* use. For *in vivo*

derivatization of non-proteinaceous species the trick can be done by taking advantage of the biosynthetic apparatus of the organisms using modified metabolic precursors.[49,50,51,52] This latter approach, however, is limited to the introduction of metabolically tolerable, small bioorthogonal motifs (e.g. azide, acetylene).

3. Imaging with bioorthogonalized light emitting markers

Species capable of releasing photons upon various means of excitation can be very different by nature. Fluorescent species that emit photons upon photoexcitation can be natural or synthetic by origin. This latter group can be further divided to organic and inorganic subcategories according to the composition of the labels. One advantage of applying synthetic probes is that their chemical and photochemical features can be synthetically tailored for the special needs.[53] Inorganic fluorophores on the other hand can be superior from the photostability and brightness point of view. Within this review, we structured our discussion by listing the groups of fluorescent markers that offer solutions to either of the obstacles faced in fluorescent bioimaging applications (i.e. autofluorescence, background fluorescence, photobleaching and brightness). Therefore we discuss NIR emitting, fluorogenic and nanoparticulate species that can be installed onto the biomolecule of interest by bioorthogonal modulation schemes. The list presented here is far from comprehensive and the readers interested in more details e.g. on nanoparticles can find excellent reviews on recent developments.[54]

3.1. Bioorthogonally applicable small, green, red and NIR emitting organic fluorophores

In general, fluorescent imaging of biological samples prefer light emitting markers with signals, clearly distinguishable from fluorescence of naturally occurring fluorophores (aromatic amino acids, DNA bases etc.). Such autofluorescence interferes the specific signals of synthetic dyes especially when their luminescence is dim. To reduce autofluorescence, therefore increase signal-to-noise ratio, several techniques emerged (e.g. time-resolved techniques). Other approaches utilize labels with large Stokes-shifts in combination with certain filters, or fluorophores that are excitable and emit at wavelengths (red, far-red, NIR regime), where natural fluorophores are not absorbing and emit photons. Visible – NIR labels are therefore the most common markers in bioorthogonal labeling schemes.

One of the very first examples for bioorthogonalized small organic probes appeared as early as 2003. In their report, Cravatt and co-workers introduced a rhodamine-alkyne probe suitable for functional proteome analysis.[55] In their activity-based protein profiling scheme a

sequential approach was followed where an active-site directed chemical modification effected by an azide-derivatized phenyl sulfonate ester (PS-N₃) was followed by a click reaction with the rhodamine-alkyne tag. This approach proved to be just as efficient and in some cases superior in terms of labeling efficiency and probe variability to the previously applied tagging schemes e.g. where a rhodamine-tagged phenyl sulfonate probe (PS-Rh) (Figure 2) was applied to tag glutathione S-transferases (GSTO 1-1). Furthermore, the smaller reagents applied in the sequential scheme are less likely affect e.g. the binding affinity of enzymes of interest. The more efficient labeling and thus, the more intense fluorescent signal observed in the case of PS-N₃ was explained by substitution of the bulky rhodamine tag for the small azide group. An even more important outcome of these experiments was that unlike previous methods, this sequentially driven activity-based protein profiling scheme could detect protein activities even in living organisms. Since then, Cravatt and co-workers have used this strategy to profile breast cancer cells [56] with a similar rhodamine probe and a bisalkynyl-naphthalene probe for tagging cytochromes P450.[57]

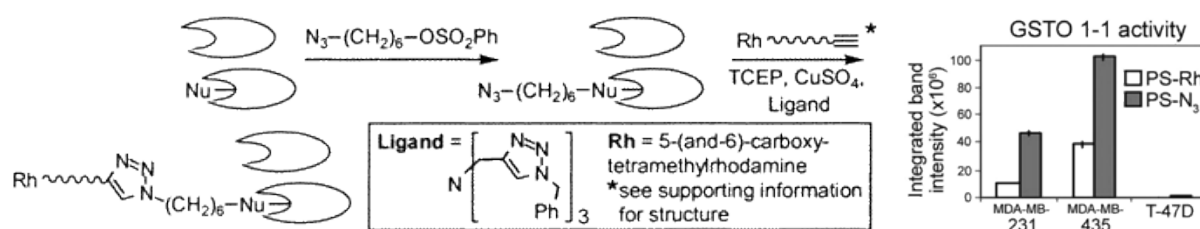


Figure 2. *In vitro* labeling of enzymes in complex proteomes by PS-Rh or PS-N₃ and GSTO 1-1 activity in human breast cancer lines measured by in-gel fluorescence scanning of labeled proteomes. [Reprinted with permission from ref 55. Copyright (2003) American Chemical Society]

In the same year, Ju *et al.*[58] proved that the azide-alkyne reaction can also be extended to tag oligonucleotides. In their account they addressed the need for the efficient and stable modification of DNA. First, they modified an oligonucleotide with an azide containing tag at the 5'-end, which was subsequently allowed to react with an alkynyl 6-carboxyfluorescein derivative in the presence of copper catalyst. The click reaction successfully demonstrated the ability to synthesize fluorescent oligonucleotides with high selectivity, yield, and stability. Such oligonucleotide constructs could be utilized for DNA analysis without further purification, and can be used directly in DNA sequencing techniques e.g. the Sanger dideoxy chain termination method.

A fluorescein-derived label suitable for the efficient preparation of homogeneous antibody-drug conjugates was introduced recently by the Boons group.[59] By remodeling the oligosaccharides of an anti-CD22 monoclonal antibody using a cytidine-monophosphate-based

sialic acid derivative, they introduced azide moieties onto the antibodies. To calculate the incorporation efficiency by fluorescence intensity measurements, a cyclooctyne-fluorescein derivative (DIBO-FITC) was used to label the azide groups by means of strain-promoted azide-alkyne cycloaddition.

Compared to commonly utilized dyes with blue-green emission, fluorophores emitting in the red or near infrared (NIR) region are more suitable for biological (*in vitro* and *in vivo*) applications as there is little or no interference from biological luminescence (autofluorescence). At the same time they enable deeper tissue imaging due to improved photon penetration distance in this portion of the spectrum (the so called ‘water-window’). The earliest examples for such NIR labels belonged to the cyanine family and are still widely used. For example, Hilderbrand *et al.*[60] used the Cy5 core and decorated it with SO_3^- groups on the one hand, to improve water solubility and an azide or alkyne motif on the other hand through a pendant linker of the polymethyne chain. Similarly to others, the suitability of this probe was tested on metabolically modulated azide-decorated glycans a method developed by Wong *et al.*[61] and Bertozzi *et al.*[22]

Hang and co-workers designed alkyne and azide functionalized photostable 2-dicyanomethylene-3-cyano-2,5-dihydrofuran frameworks with red-shifted emission (alk-CyFur and az-Cyfur) [62] to study the incorporation of azido- and alkynyl-fatty acid chemical reporters into N-myristoylated and S-palmitoylated proteins. The azido-fatty acid modulated Jurkat T cell lysates were allowed to react with alk-CyFur or alk-Rho (an alkyne-derivatized Rhodamine) under CuAAC conditions. The proteins were then visualized by in-gel fluorescence imaging. Due to the distinct spectral properties of Rho and CyFur, scanning at various excitation/emission channels allowed selective detection of the fluorophores. Moreover, the different linkages used to harbor the azide and alkyne moieties resulted in different spectral properties. For example, the ether-linked alk-CyFur showed considerably red shifted emission with a slightly higher quantum yield compared to its congener az-CyFur, where azide was linked through a carbamate. These distinct spectral properties allowed efficient Förster-type resonance energy transfer (FRET) to occur when the two CyFur probes were brought into close proximity. The FRET system showed remarkable pseudo Stokes-shift allowing far-red signal detection holding great promise in biological applications.

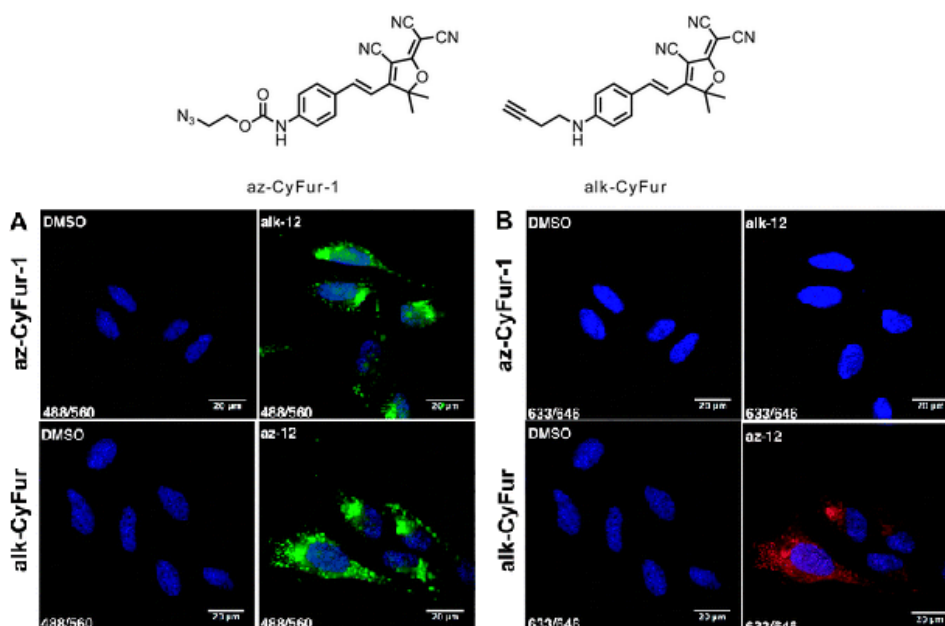


Figure 3. Top: Structures of **az-CyFur-1** and **alk-CyFur**. Bottom: Fluorescence microscopy of azido (az-12)- and alkynyl (alk-12)-fatty acid labeled HeLa cells after bioorthogonal ligation with clickable dyes. (A) Imaging with 488 nm excitation and 560 nm emission long-pass filter. Top panel: az-CyFur-1-labeled proteins. Bottom panel: alk-CyFur-labeled proteins. (B) Imaging with 633 nm excitation and 646-753 nm emission filter. Top panel: az-CyFur-1-labeled proteins. Bottom panel: alk-CyFur-labeled proteins. [Reproduced in part from Ref. 62 with permission of the Royal Society of Chemistry (RSC)]

The multi-channel, cross-talk free imaging capability of the two CyFur probes was demonstrated on HeLa cells metabolically modified with azide- and alkyne-fatty acids on their surface glycolipids (Figure 3).

The Lemke group used Cy5 and Atto532 cores both suitable for localization-based SRM techniques to construct tetrazine conjugates for dual-color pulse-chase imaging of surface insulin receptors (IR) expressed at different times.[34] They examined the reactivities of different dienophiles (simple-cyclooctyne, SCO, reactive cyclooctynes, BCN and highly reactive *trans*-cyclooctene, TCO*) with Me- and H- substituted tetrazines and found that appropriately chosen tetrazine-dienophile pairs can afford orthogonal tagging reactions (Figure 4). Their approach, dubbed selectivity-enhanced strain promoted inverse-electron-demand Diels-Alder cycloaddition (seSPIEDAC) relied on the different reactivities of simple SCO and TCO* towards the differently substituted tetrazines. The H-substituted tetrazine (H-Tet) showed high reactivity towards both dienophiles. In contrast, the Me-substituted tetrazine (Me-Tet) showed appreciable reactivity only towards the highly strained TCO* motif. To demonstrate the versatility of such orthogonal tagging schemes, insulin receptors of HEK293T cells were site-specifically modified with SCO and TCO* bearing lysine using a promiscuous orthogonal tRNA-RNA synthase (tRNA/RS) pair.

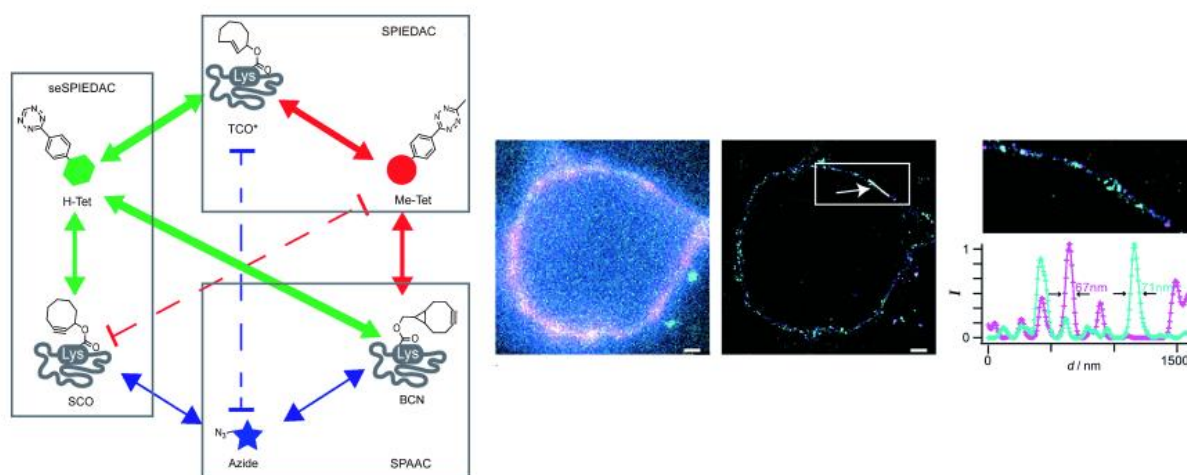


Figure 4. Left: Reactivities of TCO*, SCO, and BCN with azide (blue), H-Tet (green), and Me-Tet (red) in SPAAC, SPIEDAC, and seSPIEDAC reactions. The thickness of arrows correlates with reaction rate. Dashed lines highlight reactants that do not react with each other under the tested conditions. Right: SRM images of cells expressing IRs after seSPIEDAC labeling. Widefield (left) and SRM (middle) images of labeled IR (Atto532 in magenta, Cy5 in cyan). Right: inset from the middle panel and a line plot (across the line shown in middle panel, which is highlighted by an arrow). [Reproduced in part from Ref. 34 with permission of John Wiley & Sons, Inc. Copyright © 2014 by John Wiley Sons, Inc.]

To achieve dual-color labeling of live cells, SCO- and TCO*-modified unnatural amino acids (UAAs) were genetically encoded and incorporated into IRs by pulse–chase experiment (Figure 4) where the growth medium was first pulsed with the first UAA (TCO*-Lys) that was chased with incubation with the second UAA (SCO-Lys). The IRs were then allowed to react first with Me-Tet-Cy5 to tag TCO* moieties. Provided that all TCO* was consumed, a second labeling reaction using highly reactive H-TetTet-Atto532 probe allowed selective tagging of SCO modified IRs only (Figure 4). Dual-color localization-based super resolution microscopy (SMR) imaging of the cells revealed heterogeneous distribution of insulin receptors clusters at the membrane.[34]

Hildebrand and co-workers [31] took advantage of the orthogonality of the SPIEDAC and SPAAC reactions for selective multi-target imaging scheme (Figure 5). In their experiment two different cell types were labeled in a simultaneous double-click test. Two cancer cell line (SKBR-3 and A431, expressing different receptors) antibodies were labelled with AF567 and AF488 fluorophores on the one hand, and modified genetically either with *trans*-cyclooctene TCO or cyclooctyne DBCO, respectively on the other hand. In the next step, the co-cultured cells were first incubated with the mixtures of the antibodies, then with AF750-Tetrazine and AF647-azide probes, simultaneously. The images revealed (Figure 5) that AF750-Tetrazine and AF647-azide allowed rapid and selective labeling of TCO and DBCO modified cells, respectively (Figure 5).

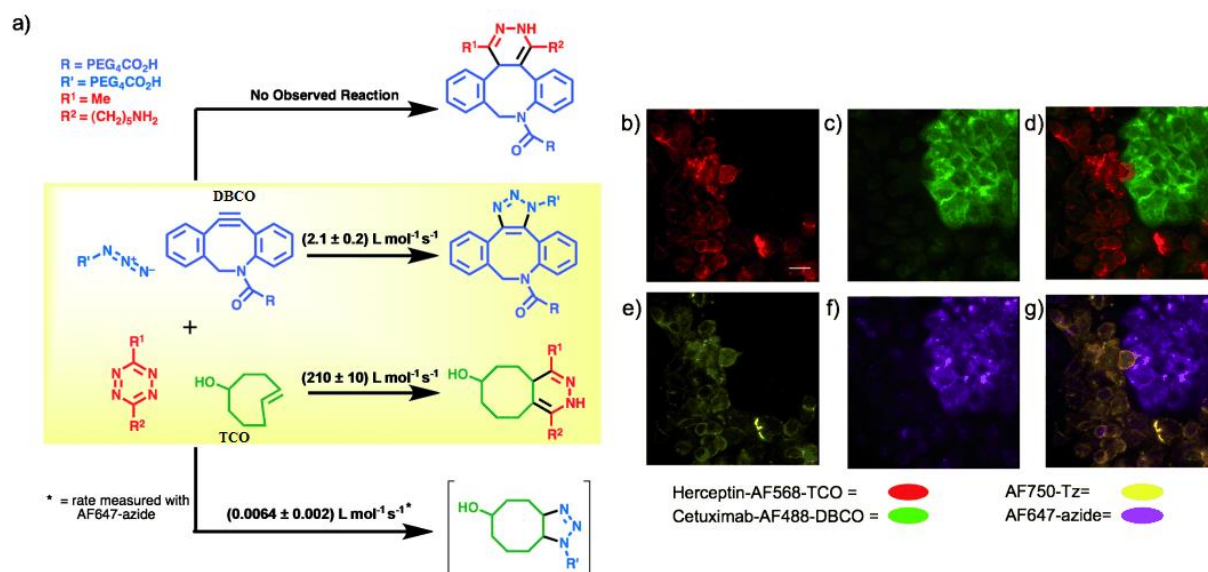


Figure 5. a) The four cycloaddition reactants and representative cycloaddition products/potential products. Second-order rate constants listed are from incubations of the two individual reactants in phosphate-buffered saline (PBS), pH 7.4 at 37 °C. The desired azide–DBCO and tetrazine–TCO–OH cycloadditions are highlighted in yellow. b)–g) fluorescence microscopy images of co-cultured A431 (EGFR+) and SKBR-3 (HER2/neu+) cells. Cells were treated with Cetuximab-AF488-DBCO and Herceptin-AF568-TCO, followed by AF647-azide and AF750-tetrazine concurrently. Shown: fluorescence from b) AF568, c) AF488, d) AF488/AF568 merge, e) AF750, f) AF647, g) AF647/AF750 merge. Scale bar in (b): 50 μm . Panels (e) and (f) show the selective covalent labeling by AF647-azide and AF750-tetrazine of Cetuximab-AF488-DBCO bound to the EGFR receptors and Herceptin-AF568-TCO bound to the SKBR-3 cells, respectively. [Reproduced in part from Ref. 33 with permission of John Wiley & Sons, Inc. Copyright © 2011 by John Wiley Sons, Inc.]

Apart from the emission wavelength, the brightness and cell-permeability are also important features of fluorescent probes. The usually low quantum yields of small organic NIR fluorophores can often be a drawback when working at low concentrations. The Johnson group addressed this problem by designing a new near-infrared silicon–rhodamine probe (SiR-tetrazine) that can be conjugated to TCO modified proteins via the SPIEDAC reaction.[63] Green fluorescent proteins expressed in *E. coli* were modified genetically with TCO- or SCO-Lys through amber (TAG) stop-codon suppression technique. TCO permits fast labelling with probes bearing tetrazines while SCO derivative was expected to be unreactive towards the particular tetrazine motif and served as a control. As supposed, successful labelling of intact *E. coli* cells was obtained exclusively for TCO, but not for SCO or wild-type GFPs. and any other protein in the *E. coli* cells did not show a red fluorescence. Moreover, due formation of a non-fluorescent lactone form in non-polar media, the SiR probe gives reduced non-specific signal that might originate from sticking to hydrophobic surfaces. These combined features make this probe ideally suited for live-cell super-resolution microscopy (Figure 6).

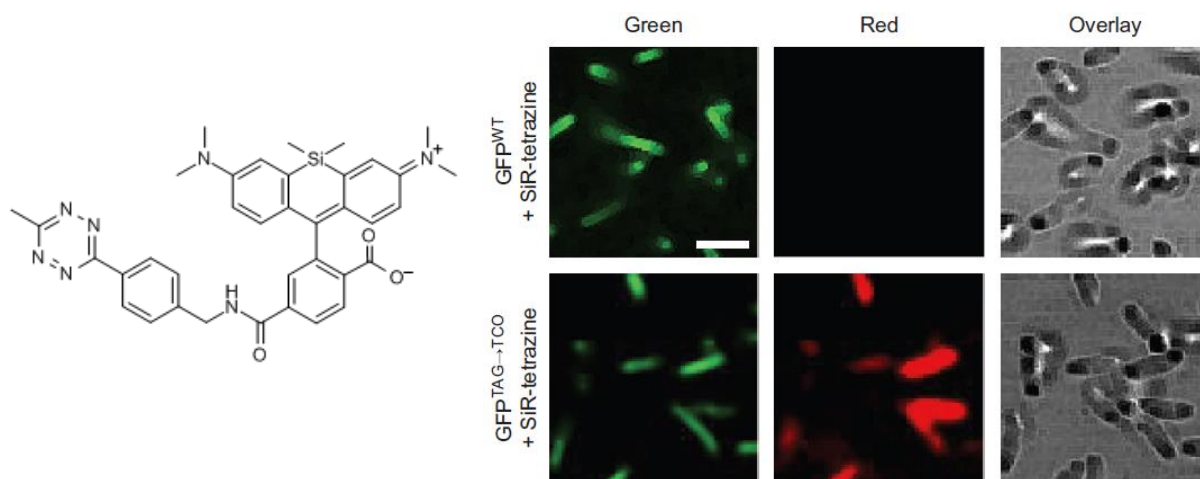


Figure 6. Left: silicon–rhodamine–tetrazine probe. Right: Live *E. coli* cells expressing GFP^{WT} (upper row) and GFP^{TAG→TCO} (lower row) were incubated with SiR-tetrazine. The cells were imaged for green or red fluorescence (third column shows the overlay). [Reprinted from Ref. 63 by permission from Macmillan Publishers Ltd: Nature Chemistry]

Cell-permeability became a profound issue of the Weissleder group during the imaging studies of Aurora Kinase A (AKA) in live cells.[64] In their initial approach, the small molecule AKA-specific inhibitor MLN8054 was decorated with a *trans*-cyclooctene (TCO) moiety, which can be visualized by a tetrazine-conjugated dye using standard, bioorthogonal two-step labeling method. *In vitro* studies using a Texas-Red-tetrazine conjugate (TR-Tz) confirmed, that the applied two-step labeling method (labeling with MLN8054-TCO and imaging with TR-Tz) is more efficient compared to direct labeling with fluorescent MLN8054-TR conjugate (IC₅₀ value of 61.8 nm versus 437.3 nm, respectively). However, TR-Tz appeared to enter cells through endocytosis, and this resulted in bright, punctate staining, which masked the localization of TR-Tz to MLN8054-TCO (13)/AKA.

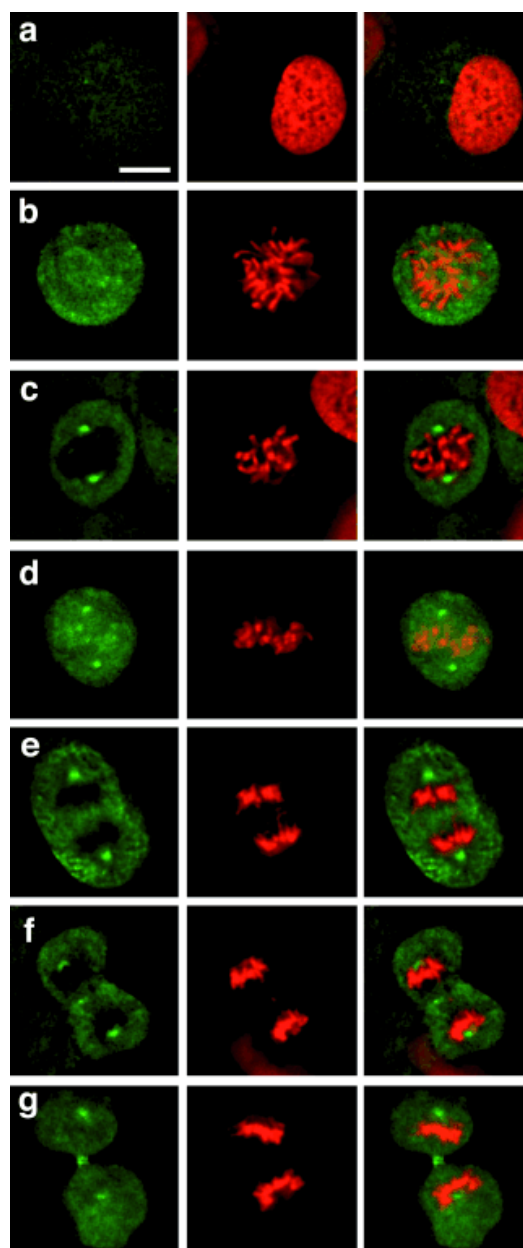


Figure 7. Localization of MLN8054-TCO (13)/CFDA-Tz in dividing HT1080 H2B-Apple cells. HT1080 cells were incubated for 30 min with 125 nm MLN8054-TCO (13), washed and incubated for 30 min with 1 μ m CFDA-Tz for bioorthogonal reaction inside living cells. Following 2 h of washing, live cells at different stages of mitosis were imaged at 40 \times with 1.6 zoom by deconvolution microscopy. Left column: MLN8054-TCO (13)/CFDA-Tz, Middle column: H2B-Apple, Right column: merge. a) Interphase, b) Prophase, c) Prometaphase, d) Metaphase, e) Anaphase, f) Telophase, g) Cytokinesis. Scale bar: 10 μ m. [Reproduced from Ref. 64 with permission of John Wiley & Sons, Inc. Copyright © 2012 by John Wiley Sons, Inc.]

To overcome this limitation, the group screened a library of various Tz modified fluorophores to identify a probe capable of diffusion-mediated cellular uptake. For this screening process a modified PANC-1 cell-line expressing mCherry-AKA (RFP-AKA) was used as probe target. The best candidate proved to be carboxyfluorescein diacetate-Tz (CFDA-Tz), which was further investigated in the two-step labeling procedure, using the same RFP-

AKA expressing PANC-1 cell-line. Final *in vivo* experiments on live, actively dividing cells were performed using an HT1080 fibrosarcoma cell-line stably transfected with H2B-Apple (a red fluorescent protein). Labeling of the endogenous AKA during different stages of the G2/M phase with MLN8054-TCO / CFDA-Tz showed very good correlation with the expected localization of AKA during mitosis (Figure 7).

Compared to the traditional dyes, the decreasing quantum yield in the NIR region also poses a challenge. Zumbusch *et al.*[65] examined this problem and synthesized a new family of Pyrrolopyrrole Cyanines (PPCy) dyes with extremely narrow NIR absorption and emission bands with excellent quantum yields (Figure 8). Achilefu and co-workers [66] incorporated two alkyne moieties into the same core. Alk-PPCy showed similar characteristics and its azide-clicked triazole derivative showed large extinction coefficients ($\epsilon = 138\,000\text{ M}^{-1}\text{cm}^{-1}$) and quantum yields ($\phi = 37\%$ relative to ICG in DMSO). They also examined the photostability of the PPCy dyes and found that it can withstand the intense light used in microscopy. In contrast, most NIR carbocyanine dyes rapidly bleach under these conditions, which prevents their use in time-lapse microscopy (Figure 8).

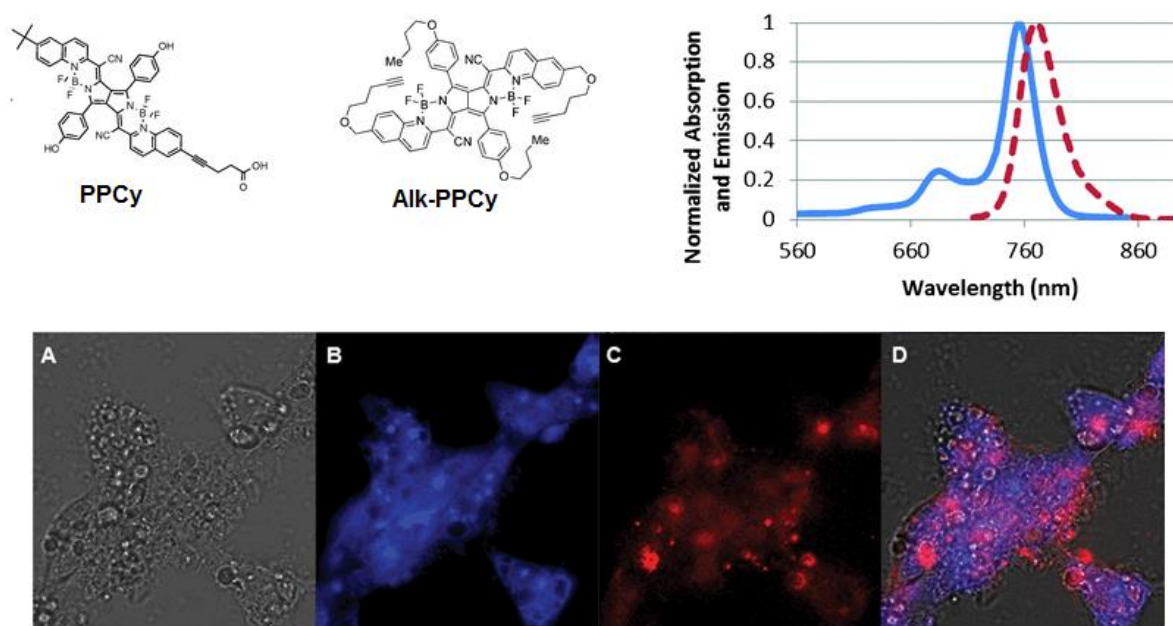


Figure 8. Top: Structure of **PPCy** dye and its bioorthogonalized **Alk-PPCy** derivative with normalized absorption and emission spectra. Bottom: Live cell imaging using **Alk-PPCy**. MCF-7 cells were incubated with **Alk-PPCy** (5 μM) in DMEM containing 0.03% DMSO, 0.3% Tween80 and GeneJuice (5 μM) at 37 $^{\circ}\text{C}$ for 18 h. (A): Bright field; (B): TOTO1 stained cell nuclei; (C): **Alk-PPCy** stained cell; (D): composite image of the cells with TOTO1 and **Alk-PPCy** staining. [Reproduced in part from Refs. 65 and 66 with permission of The Royal Society of Chemistry (RSC)]

Another common issue in fluorescent imaging techniques, especially in FRET applications is the small Stokes-shift of the probes. Kele and co-workers [67,68] synthesized a

series of dyes with large Stokes-shifts based on a stilbene motif (Figure 9). The labels were furnished with alkyne and/or azide as a bioorthogonal functionality and their emission ranged from 630 nm to 805 nm, covering the spectra from the red to the NIR regime. The dyes were tested in similar conditions mentioned previously, i.e. in the labeling scheme of azido-mannose modified surface glycans of CHO cells.

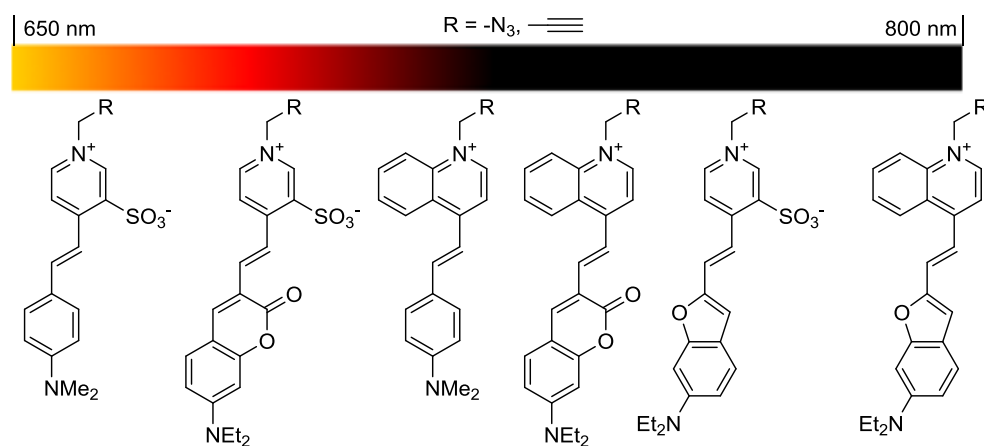


Figure 9. Structure of the “clickable” dyes with large Stokes-shifts.

Fluorophores exhibiting large Stokes shifts make these dyes ideal candidates for Förster-type Resonance Energy Transfer (FRET) applications, since direct excitation of acceptor emission by the light used to excite the donor is an often encountered problem in FRET assays. The possibility to use a NIR fluorescent probe to monitor the release of Daunomycin (Dau), a fluorescent anticancer drug was also demonstrated by the Kele group, [68] on a dually labeled, model peptide motif, that could be cleaved by an enzyme. The experiments showed that the fluorescence of Dau was efficiently quenched by an appropriately chosen dye, and the fluorescence of Dau could be fully reinstated upon hydrolysis of the dually labeled tetrapeptide-based enzyme substrate. In another study [69], the emission intensity of these dyes showed remarkable dependence on local polarity and showed large fluorescence increase when conjugated to oligonucleotides. Upon hybridization with the respective counterstrands it also became apparent that a special focus must be put on the design and location of the linker between the oligonucleotide and the dye.

3.2. Bioorthogonal fluorogenic probes

In bioorthogonal labeling schemes larger or smaller excess of the fluorescent label is needed to facilitate tagging efficiency as the required probe concentration is directly proportional to the reaction rate of the applied bioorthogonal chemistry. For example, relatively

slow Staudinger ligation schemes require mM concentration of the label, whilst SPIEDAC reaction allow probe concentration in the nanomolar range. In cases where larger concentration of the probe is applied the excess of the fluorescent label has to be removed via several washing step cycles to minimize background fluorescence of the unreacted probes. Another approach to minimize background fluorescence relies on the use of so-called fluorogenic (also known as turn-on, or smart) probes. These fluorogenic labels have the unique feature of becoming fluorescent only upon reaction. Such fluorogenic dyes are extremely advantageous in *in vivo* labeling schemes where washing steps are undesirable.

Amongst the various fluorogenic probes bioorthogonally applicable scaffolds are of special importance as they can ensure site-specific tagging of the biomolecules of interest. There are two major approaches that rely on the use of bioorthogonal handles. There are instances where the bioorthogonal function is responsible for the quenching effect and upon chemical transformation the fluorescence is enabled. Other approaches use the bioorthogonal transformation to trigger the release of either photocaging or quencher moieties. Whichever mechanism is responsible for the low emission intensity of the quenched forms the outcome after bioorthogonal reaction is the enhancement of fluorescence intensity. Therefore the most important feature of such fluorogenic systems is their enhancement factor (EF), which is given by the ratio of either the intensities, the quantum yields or brightnesses of the product and the starting material, respectively at a given wavelength. Other features such as brightness, excitation and emission maxima in the red-NIR regime, photostability or membrane permeability are also preferred. Within this chapter we will follow a reaction-based discussion to give an insight into the recent developments on bioorthogonally applicable fluorogenic probes.

3.2.1. Azide-bearing fluorogenic dyes

Azide modified fluorescent scaffolds are one of the most common and widely used bioorthogonally applicable fluorogenic probes. The azide group is highly energetic, yet very stable under a variety of conditions. Its selective reactivity towards phosphanes and (cyclo)alkynes makes it exceptionally useful in bioorthogonal labeling applications.[17,70,71] Further advantages are its easy accessibility (e.g. from amines) and relatively small size, which minimally perturbs the biological systems.

There are diverse mechanisms to explain the quenching effect of the azide moiety. In their respective work Wang et al. accuse the electronrich α -nitrogen of the azide for the

quenching.[72] Kele and co-workers used quantum chemical calculations to investigate the quenching effect posed by the azide. They found that the presence of the azide opens alternative, non-radiative relaxation channels.[73] In other instances PET mechanism can be the possible cause for non-radiative relaxation.[74]

One of the very first reports on bioorthogonally applicable small fluorogenic dyes introduced a series of 3-azido-coumarin derivatives (Figure 10, **1**), some of which showed remarkable EF in water/DMSO mixture.[72] Of these azidocoumarins 3-azido-7-hydroxicoumarin (AHC), was found to be especially useful and found wide range of fluorogenic tagging applications. It shows 100-fold increase in fluorescence intensity (in ethanol - water). In their work, Zong *et al.* incorporated the fluorogenic AHC scaffold into a dendrimer.[75] This fluorogenic platform was used to profile cellular proliferation by following the incorporation of 5-ethynyl-2'-deoxyuridine into newly synthesized DNA. Very recently the Dirksen group developed a method for parallel synthesis and fast screening of anti-Angiopoietin-2 peptide antibody conjugates.[76] They used 3-azido-7-hidroxi-coumarin to detect the residual, unreacted scaffolds through SPAAC.

Photoinduced electron transfer based quenching mechanism can be tracked down in the 9-azidomethyl anthracene (Figure 10, **2**) scaffold introduced by Wang and co-workers.[77] They reached 75-fold increase in emission intensity (in DMSO), and successfully applied this probe in the labeling of alkyne-derivatized cowpea and tobacco mosaic viruses using CuAAC. Seela and co-workers used the same azido-anthracene scaffold to label oligonucleotides to study duplex formation.[78] The same researchers reached high density functionalization and cross-linkage formation between alkyne functionalized DNA strands, using mono- and bis-azido-anthracenes.[79] Although the probes showed excellent fluorogenic properties its UV excitability limited its use in cellular environments.

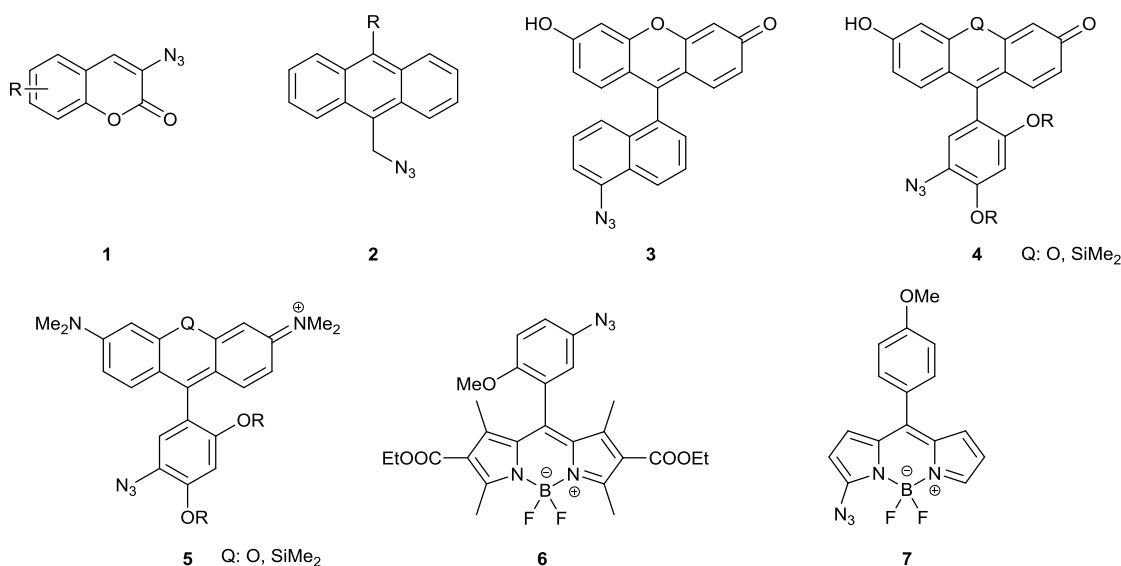


Figure 10. Various azide-bearing fluorogenic dyes based on coumarin, anthracene, xanthane and BODIPY cores.

Based on the general consideration and theoretical calculations of Nagano *et al.* [74,80] the Bertozzi group showed that the PET based quenching mechanism can be harvested in the design of new xanthane smart probes. In their account the newly reported (silica)fluorescein and (silica)rhodamine fluorogenic azides (**3-5**)[81, 82, 83] showed 35- 243-fold increase in Φ_F (PBS pH 7.4) (Figure 10). They also showed that the possible decomposition of the azide moiety to amine, a common problem in fluorogenic labeling schemes in biological systems,[84] does not contribute to unwanted background fluorescence as the respective amines had lower Φ_F than the corresponding azides. Moreover, the excitation and emission maxima of these new probes were found to be in the visible region for the fluoresceins (λ_{exc} 500 nm, λ_{em} 521 nm, PBS 7.4) and for rhodamines (λ_{exc} 561 nm, λ_{em} 583 nm, PBS 7.4) and in the far red/near infrared regime for Si-fluoresceins (λ_{exc} 591 nm, λ_{em} 609 nm, PBS 7.4) and Si-rhodamines (λ_{exc} 657 nm and λ_{em} 674 nm, in PBS pH 7.4). One of the fluorescein derivatives was successfully tested in the labeling of cell surface glycans of fixed CHO K1 cells previously treated with peracetylated N-(4-pentynoyl)-mannosamine (Ac₄ManNA1, Figure 11). They also highlighted the remarkable resolution that was obtained without any washing step. A Si-rhodamine smart-probe was successfully tested using the previously described CHO K1 system together with alkyne functionalized HEK 293T cells in glycan labeling studies. Furthermore, bacteria (*E.coli*) expressing alkyne modified peptidoglycans were also labeled using SPAAC chemistry. Besides their glycan labeling properties, a set of these dyes was also tested for DNA or RNA labeling

capabilities in HEK 293T cells and in *E. coli* using 5-ethynyl uridine or 5-ethynyl deoxyuridine as chemical reporter units.[84]

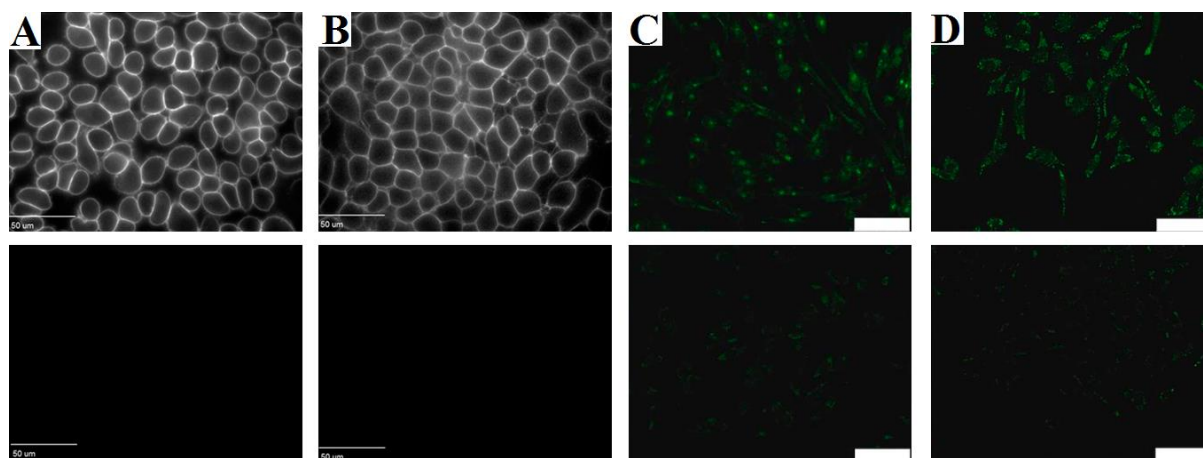


Figure 11. No-wash mammalian cell surface labeling. Upper row: treated with azido-sugars, bottom row: treated without azido-sugars as a control. Fluorescence images of CHO K1 (A) and HEK 293T (B) cells treated with Ac₄ManNAI and labeled with **4**. [[Reprinted with permission from Ref. 82 Copyright (2014) National Academy of Sciences, USA.]

Fluorescence images of CL1-5 cells treated with Ac₄ManNAI (C) or Ac₄GlcNAI (D) and labeled with **5**. [Reprinted with permission from Ref 85. Copyright (2014) American Chemical Society]

The PET-based quenching mechanism motivated Wong and co-workers to introduce an azide modified BODIPY fluorogenic dye (Figure 10, **6**) exhibiting 52-fold EF (in EtOH) upon reaction.[85] The excitation and emission maxima of the BODIPY-fluorogenic label in ethanol were λ_{exc} 501 nm and λ_{em} 515 nm, respectively. They also experienced that the potential by-product amine derivative is virtually non-fluorescent therefore it has no contribution to the background signal. A selected compound was first evaluated in alkyne-functionalized BSA tagging using CuAAC scheme, then used to label proteoglycans in fixed CL1-5 lung cancer cells, previously incorporated peracetylated alkynyl-*N*-acetylmannosamine (Ac₄ManNAI) and alkynyl-*N*-acetylgalactosamine (Ac₄GalNAI) (Figure 11).

Wang and co-workers in 2012 reported another azido-BODIPY derivative (Figure 10, **7**), which showed an excellent, 800-fold (although in CHCl₃) increase in fluorescence intensity upon reaction with alkynes (reaction with different alkynes: λ_{exc} 514-522, λ_{em} 529-538, in MeOH).[86] KB cells overexpressing folate receptors were treated with terminal alkyne modified folate. The modified folate receptors were then successfully profiled using the azido-BODIPY derivative. However, they noticed that the negative control also showed fluorescence. The low stability of azido-BODIPY dye under the applied conditions, thus a fluorescent decomposition product was accounted for the high background signal. The authors suspected

an ICT-based mechanism behind the quenching effect. Later, Talukdar and co-workers published a similar azide modified BODIPY probe (reaction with different alkynes: λ_{exc} 502-540, λ_{em} 528-650 nm, HEPES pH 7.4), which showed 532-fold fluorescence enhancement (HEPES 7.4) upon CuAAC reaction with alkynes.[87] The authors assumed a PET-based quenching effect responsible for the fluorogenic behavior. They found that a membrane permeable cholesterol modified probe showed exclusive accumulation in the intracellular membranes. This fluorogenic-cholesterol can be used to follow cholesterol trafficking in live cells.

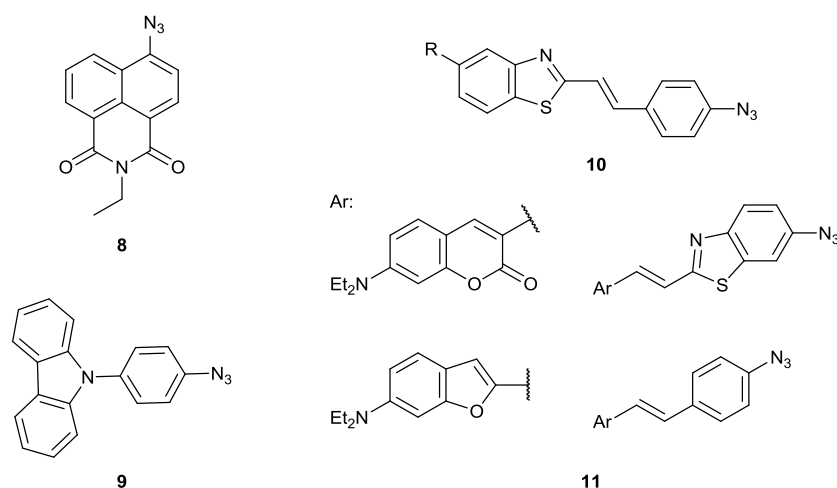


Figure 12. Various azide-bearing fluorogenic dyes based on 1,8-naphthalimide, carbazole and stilbene cores.

Most probably not PET based quenching mechanism is responsible for the fluorogenic nature in a 4-azido 1,8-naphthalimide fluorogenic dye (Figure 12, **8**) emitting in the blue region (λ_{exc} 357, λ_{em} 422 nm, PBS pH 7.2).[61] The authors found that the probe shows excellent fluorogenic properties (about 100-fold EF). Together with other fluorogenic azido-dyes, this azido-naphthalimide was also successfully applied in the real time activity measurement of aberrantly activated oncogenic Src kinases in the crude lysate of leukemia cells.[88]

Just very recently, an azido-phenyl carbazole (Figure 12, **9**) was introduced by Bräse and co-workers.[89] This carbazole derivative was found to be virtually dark, while fluorescent after reaction with alkynes, possessing UV excitability (291-293 nm, various solvents) and visible emission (387-492 nm, various solvents). The triazolic products showed strong pH dependency both in terms of emission wavelengths and Stokes-shifts. Theoretical calculations and experimental results indicated that a twisted internal charge transfer (TICT) is responsible for the photophysical properties of these new dyes. Two conjugates were further tested in HeLa

cells as a polarity sensitive probes. It was found that both derivatives were quite stable under live cell conditions and they showed strong preference to the endosomal-lysosomal system. The authors therefore foresee them as promising probes to follow endocytotic uptake processes.

In 2013 Kele and co-workers reported on the design and synthesis of a set of new, azide-bearing fluorogenic dyes (Figure 12, **10**) based on the stilbene motif.[73] Theoretical investigations suggested that fast rotation and bending of the azide group opens up the possibility of the internal conversion of the two lowest excited states followed by another internal conversion process to the ground state. They used the same calculation model to predict fluorogenicity and designed another set of stilbene type of azide-bearing fluorogenic dyes (Figure 12, **11**) with red-shifted excitation and emission properties. [90] The dyes were tested in live *E.coli* cultures to target genetically encoded cyclooctyne motifs in proteins. The proteins were then successfully profiled in cell-lysates.

3.2.2. (Cyclo)alkyne fluorogenic dyes

The presence of an alkyne motif can also function as a quencher although in rarer instances. Since metabolic, or genetic incorporation of azide-modified chemical reporters is well developed, such alkyne-bearing fluorogenic probes would be obvious targets of probe research. However, alkyne-based quenching is less generalizable and rather restricted to a few special cases. Following this pioneering work on terminal alkynes,[91] Bertozzi and co-workers reported on the design and synthesis of a coumarin-fused cyclooctyne derivative (Figure 13, **12**).[92] The probe showed moderate, 10-fold increase in quantum yield upon conjugation (λ_{exc} 305, λ_{em} 438 nm, PBS pH 7.4) with azides. Following this track, Boons and co-workers introduced another fluorogenic cyclooctyne (Figure 13, **13**), which shows better EF ratio (60-fold for Φ_F , 1900-fold for brightness, λ_{exc} 362-364, λ_{em} 489-499 nm, MeOH).[93] Moreover, the stability of this latter label under acidic and basic media was found to be remarkable. Theoretical investigations suggest that the difference in emission intensities is due to the substantial differences in oscillator strengths of the $S_0 \leftrightarrow S_1$ transitions in the planar C_{2v} -symmetric **13** compared to the symmetry-broken and nonplanar triazolic product.

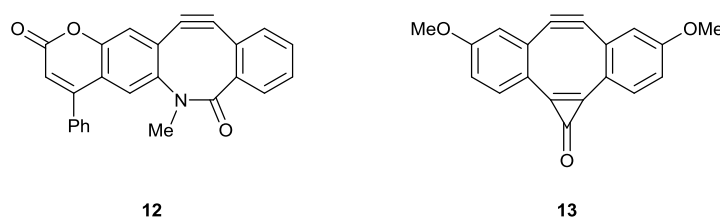


Figure 13. Fluorogenic dyes based on cyclooctyne motifs

3.2.3. Fluorogenic probes for Staudinger ligation

As it was outlined in the introduction, during the course of the Staudinger ligation the aza-ylide intermediate formed in the reaction between azides and phosphanes is captured by a neighboring electrophilic trap, mostly an ester group, leading to the overall formation of an amide and a phosphane oxide, while releasing a molecule of alcohol.[1] These characteristics are exploited when fluorogenic Staudinger ligation probes are designed. There are examples where the original phosphane is responsible for the quenching via ICT. Upon oxidation to the phosphane oxide the ICT originating from the phosphorous' lone pair is no longer possible, therefore the fluorescence reinstates. An example for this approach is presented by Bertozzi *et al.*[94] Their coumarin-modified phosphane (Figure 14, **14**) showed 60-fold fluorescence increase upon transformation to **15** (Φ_F , λ_{exc} 443, λ_{em} 495 nm, PBS) with kinetics, comparable to general Staudinger reaction ($k = 1.5 \times 10^{-3} \text{ M}^{-1}\text{s}^{-1}$ in water-MeCN 1:1). To demonstrate the versatility of this approach, they used this phosphane dye in combination with recombinant azidohomoalanine containing murine dihydrofolate reductase.

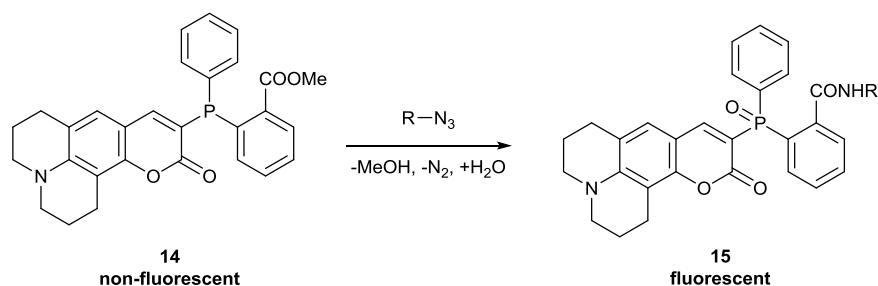


Figure 14. Coumarin based fluorogenic dye activated by Staudinger ligation. [Reprinted with permission from ref 94. Copyright (2003) American Chemical Society]

Unfortunately the phosphanes tend to oxidize spontaneously, which, in this particular case would result in increased background fluorescence. Another approach that eliminates this latter problem relies on the elimination of the alcohol. In such instances the alcohol is part of a quencher that diminishes fluorescence via FRET processes. After the ligation process the quencher is released and the fluorescence of the original fluorophore is restored.

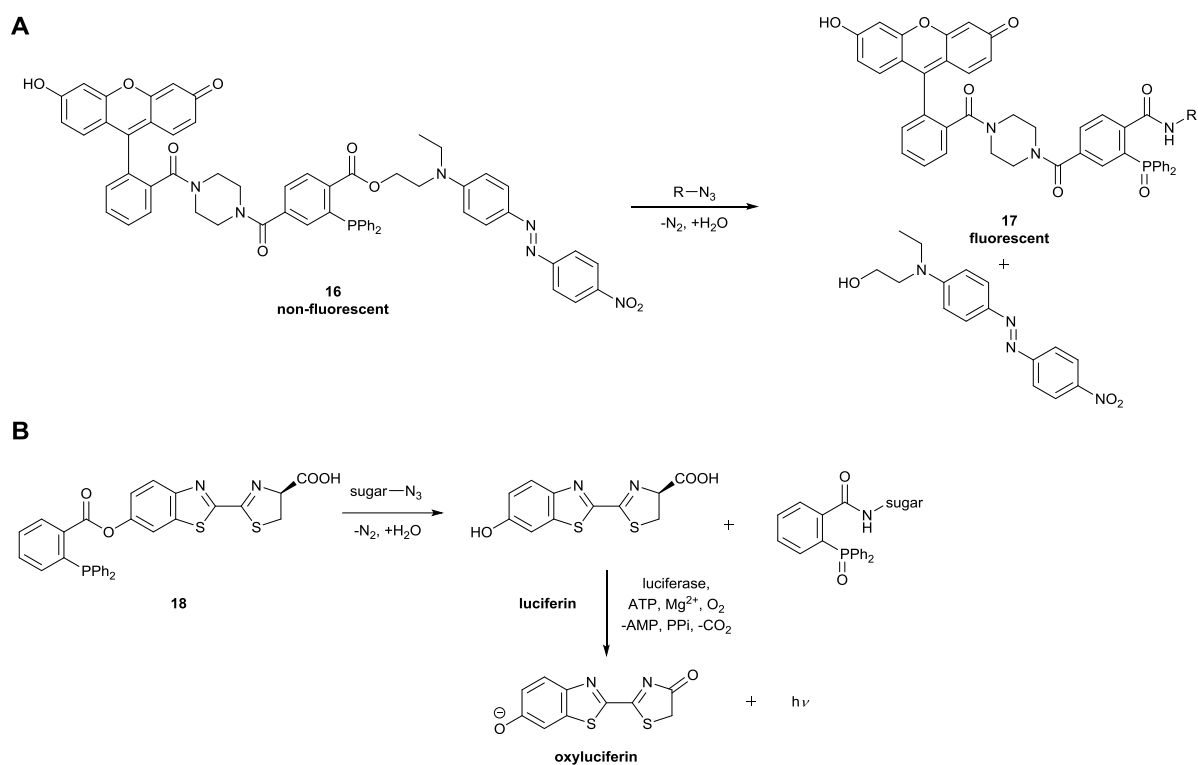


Figure 15. Fluorescence activation through Staudinger ligation. A: release of quencher from fluorescein through ester cleavage. B: release of caged luciferin for luciferase-luciferin reaction.

Not only are bond cleavage based techniques popular design elements in fluorogenic species, but it is also frequently applied in techniques involving controlled drug release.[95] Depending on the nature of the substituent on the electrophilic trap (ester, carbonate or carbamate) the released group can either be an alcohol or an amine.[96,97] Using this approach a fluorescein-Disperse Red system (**16**) was introduced by the Bertozzi group.[98] Such design afforded 170-fold increase in Φ_F after release of the quencher (**17**) (Figure 15A). This probe was tested on the well-established CHO cell-system exposing azidosialate motifs in their cell-surface glycans (Figure 16). Though the probe was quite efficient in the visualization of surface glycans it had decreased permeability, which limits its use in the imaging of intracellular targets.

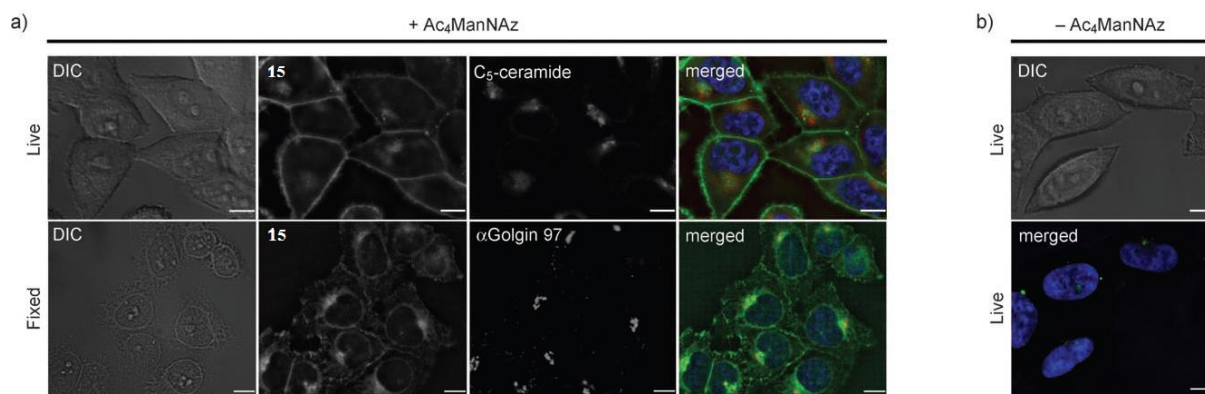


Figure 16. Fluorescence microscopic images of Ac₄ManNAz-treated HeLa cells labeled with phosphane **16**. a) Top row: Live HeLa cells treated with Ac₄ManNAz, **16** (FITC channel), and the live-cell Golgi marker BODIPY TR C₅-ceramide (Cy3 channel); bottom row: HeLa cells treated with Ac₄ManNAz, **16**, then fixed, permeabilized, and treated with anti-Golgin 97 mouse mAb and goat anti-mouse IgG-Alexa Fluor 647 (Cy5 channel). b) Live HeLa cells treated with **16** only. All cells were treated while alive with nuclear stain Hoechst 33342 (DAPI channel) and viability stain propidium iodide (Cy3 and Cy5 channels). The lack of nuclear fluorescence in Cy3 and Cy5 channels indicates propidium iodide exclusion from cells. The scale bars represent 10 μ m. [Reprinted with permission from Ref. 98 Copyright: John Wiley and Sons]

A unique combination of Staudinger ligation and bioluminescence was reported by the same group by the introduction of a phosphane caged luciferin (Figure 15B, **18**).^[99] Upon reaction with surface glycan azides a luciferin is degraded from the probe, and becomes accessible for co-expressed luciferase to produce bioluminescent signal. The method does not require external irradiation due to enzymatic activation (bioluminescence), making it a powerful imaging tool with exclusive signal-to-noise ratio.

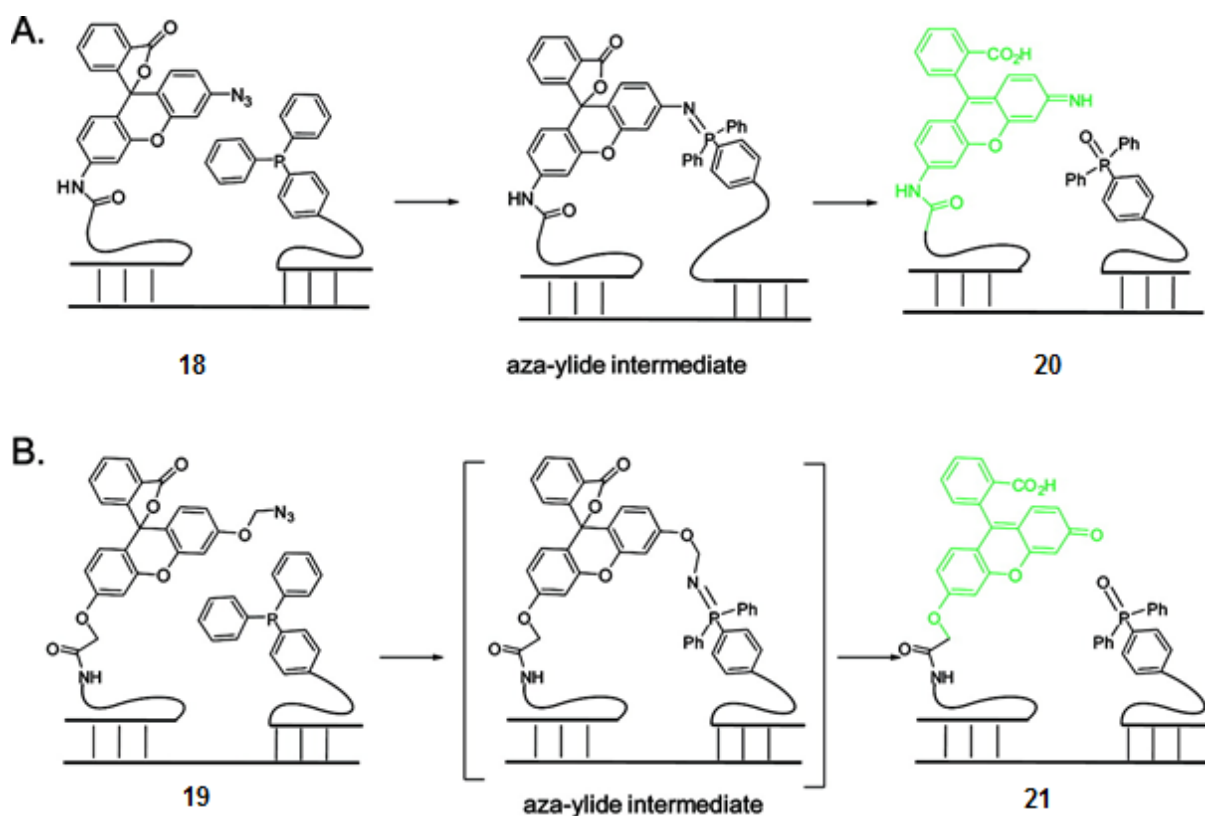


Figure 17. Fluorescence turn-on of RNA-bound azide quenched xanthenes through Staudinger reaction. [Reprinted with permission from Ref. 100 Copyright (2009) American Chemical Society]

Other approaches also harvested the potential of the original Staudinger reduction. In one of such examples the azide served as a quencher of different fluorescent xanthane cores. Upon phosphane mediated reduction of the azide moiety in constructs **19** and **20** to amines **21**, **22**, the fluorescence intensities increased considerably (Figure 17). The technique was applied to the detection of endogenous RNAs in living human cells.[100,101] In their approach two oligonucleotide templates labeled with azido-xanthane and phosphane, respectively were allowed to anneal with target RNA. Upon matched hybridization the azide and the phosphane tagged strands were brought into close proximity therefore Staudinger reduction could take place leading to strongly fluorescent products (Figure 17).

3.2.4. Photoinduced reaction of tetrazoles

The reaction originally described by Huisgen and co-workers in 1967 between 2,5-diphenyltetrazole and methyl crotonate,[102] was found to be quite useful in bioorthogonal schemes and triggered the development of a series of new tetrazoles (**23**) for bioconjugation and fluorescence imaging applications.[14] The inherent fluorogenic nature of this reaction makes this transformation quite attractive. In their very first reports Lin *et al.* used UV light (305 nm) to induce photorelease of nitrogen and formation of the reactive dipolar nitrile imine

species (Figure 18, **24**). Subsequent efforts shifted the wavelength of photoreaction together with the excitation and emission maxima of the pyrazoline (**25**) products towards the visible region through ‘scaffold hopping’ strategy (Figure 18).[12,13,16,103] These efforts resulted in photoinduction of tetrazoles in near UV and far red region (up to 390 nm and 700 nm using two-photon absorption) and the corresponding pyrazoline derivatives showed fluorescence upon visible excitation in the orange-red region (λ_{exc} 402-437, λ_{em} 575-644 nm, MeCN-PBS 1:1 v/v).[103] Reactions using cyclopropene as dipolarophile were carried out on genetically modified mammalian cells to prove the excellent efficiency and spatiotemporal control of this labeling scheme.[104] A unique framework (Figure 18, **26**) allowing intramolecular photo-click reaction was also developed and conjugated to a microtubule-binding taxoid core. This construct was applied in fluorogenic visualization of microtubules in live CHO cells (Figure 19, λ_{exc} 330-358, λ_{em} 528-617 nm, 21-112-fold increase in fluorescence emission, MeCN-PBS 1:1 v/v).[105]

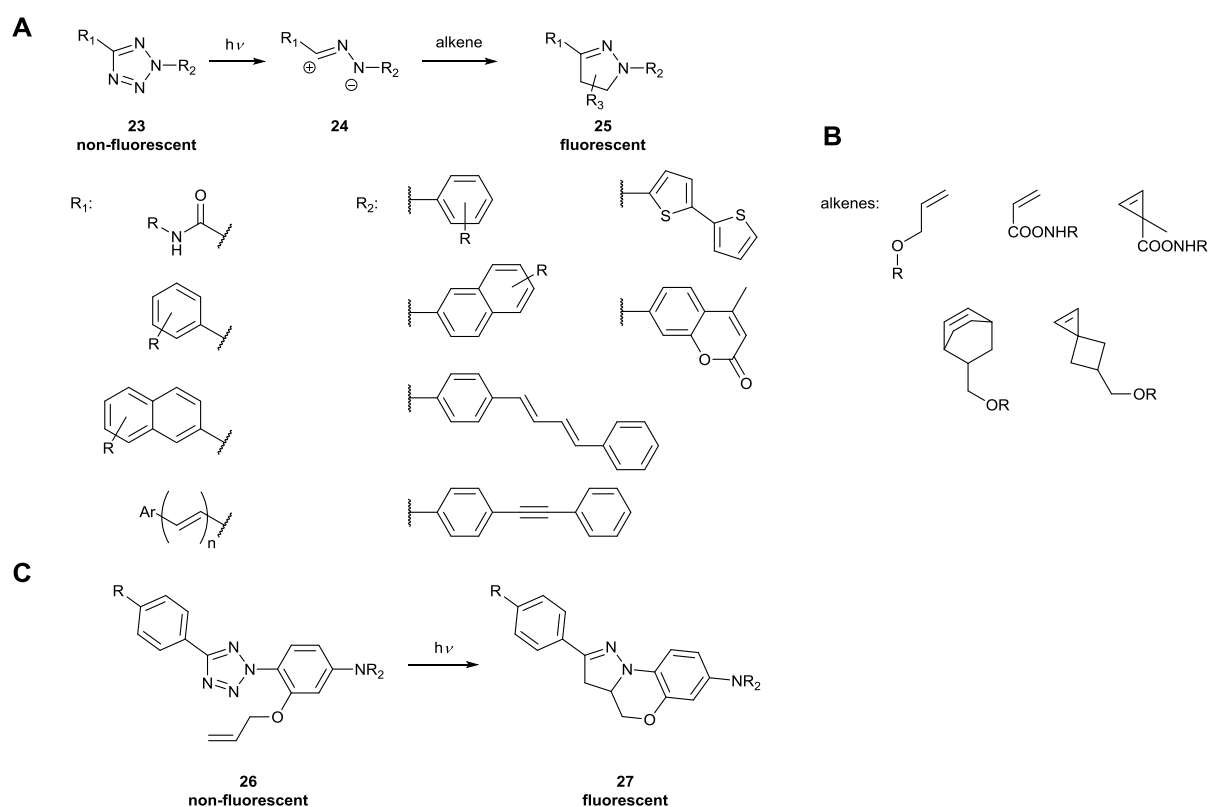


Figure 18. Tetrazole based fluorogenic dyes. A: Various dyes for photoinduced reaction. B: Commonly used alkene partners for cycloaddition. C: Reagent for intramolecular photoclick reaction.

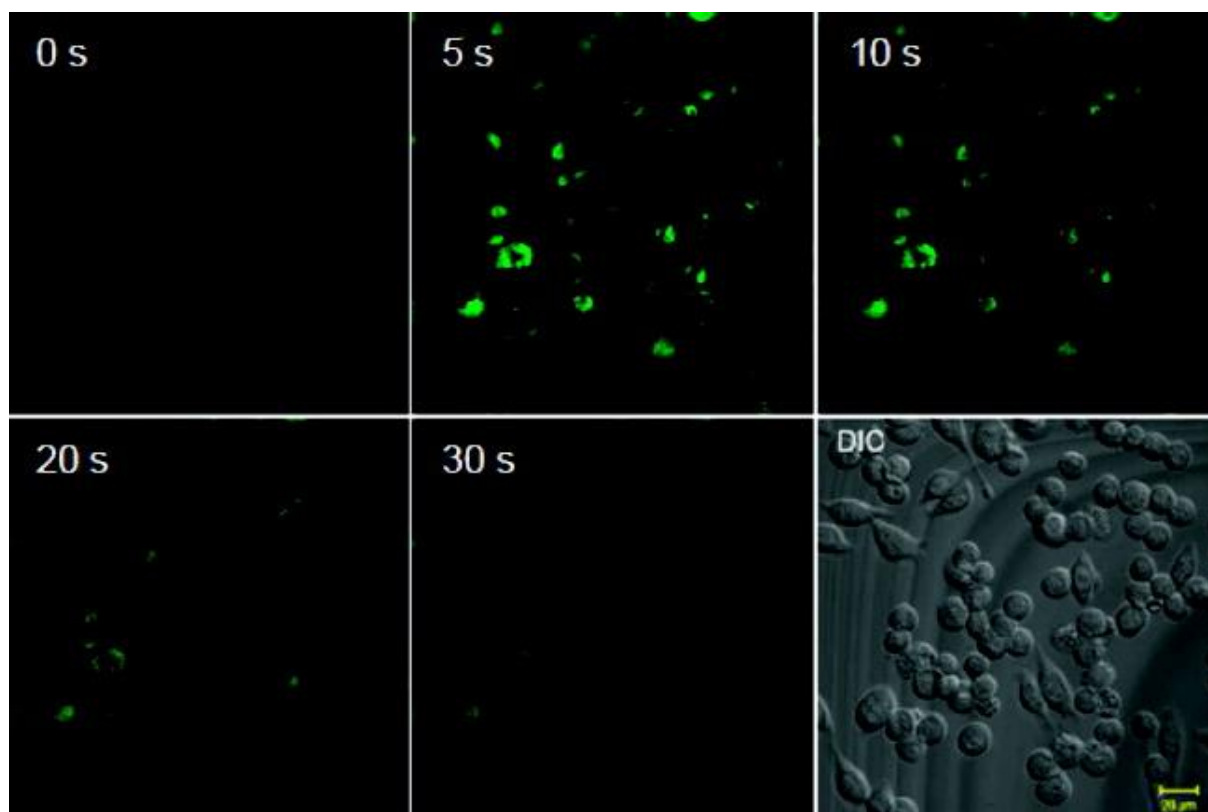


Figure 19. Time course of the photoactivation of taxoid conjugated with tetrazole **26** in live CHO cells. (a) Time-lapsed confocal micrographs of tetrazole-treated CHO cells after photoillumination, scale bar = 20 μm . Cells were treated with 1 μM of taxoid-tetrazole for 30 min before photoillumination. ZEISS filter set #49 was used for incident light filtering; for fluorescence, $\lambda_{\text{ex}} = 405 \text{ nm}$. [Reprinted with permission from Ref. 105 Copyright (2011) American Chemical Society]

3.2.5. Inverse electron demand Diels–Alder reaction of tetrazines

As described earlier, the tetrazine moiety can participate in fast and efficient strain promoted inverse electron demand Diels-Alder cycloaddition (SPIEDAC) based ligation schemes with various dienophiles. Only very recently was the quenching ability of tetrazine scaffolds harvested in fluorogenic probe designs.[106] Tetrazines can quench the fluorescence of fluorescent scaffolds with matching emission bands by traditional FRET mechanisms. Most tetrazines absorb light at around 520 nm, so virtually any fluorescent scaffolds with overlapping emission bands are suitable energy donors. Weissleder and co-workers demonstrated this using a series of green to red emitting BODIPY (**28**) and xanthane (Oregon Green) (**29**) derivatives (Figure 20). Reaction with *trans*-cyclooctene (TCO) resulted in 1.0 – 20 fold EF in PBS. To evaluate the performance of these fluorogenic dyes in more challenging media they were tested in the labeling of the microtubular network of PtK2 cells using a microtubule binding TCO-modified taxol derivative. Successful imaging of the microtubular network revealed the suitability of this approach in *in vivo* imaging schemes (Figure 21). Other research groups

developed Oregon Green and BODIPY tetrazine conjugates (Figure 20, **30**, **31**), and examined their applicability and characteristics (e.g. permeability, stability) in the labeling of RNA,[107,108,109] proteins,[110,111,112] and phospholipids[113] in details.

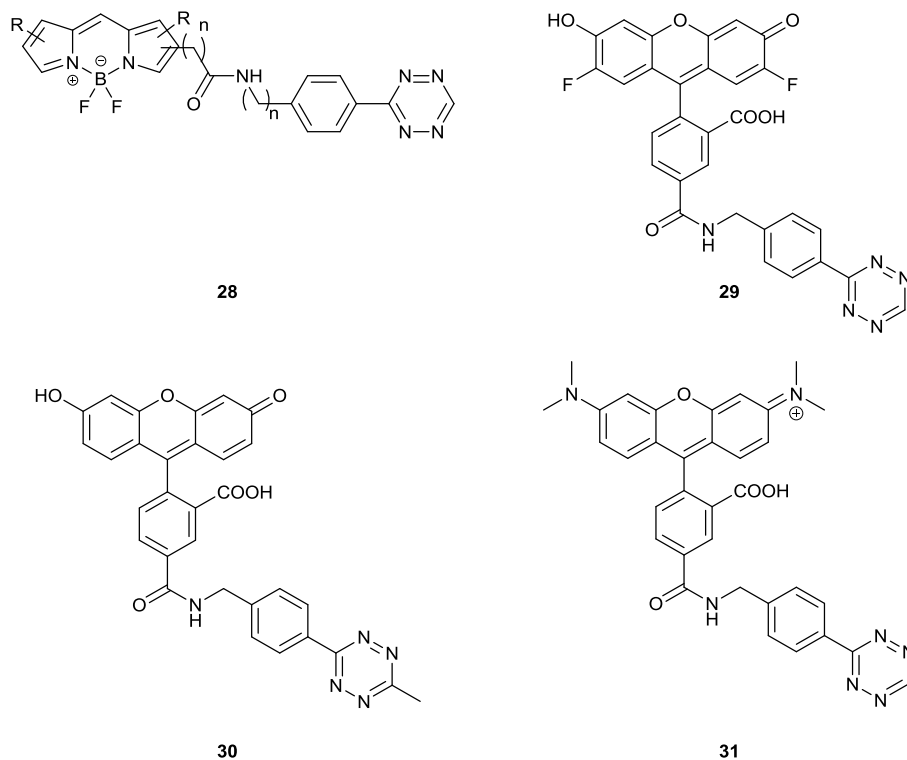


Figure 20. FRET-based tetrazine quenched fluorogenic dyes with flexible linkers.

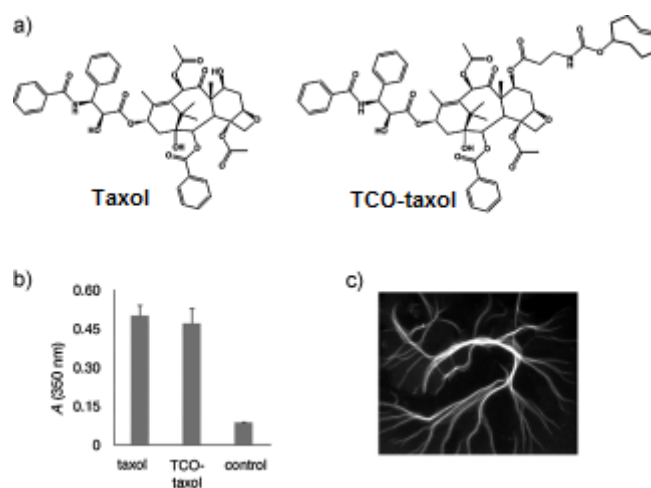


Figure 21. a) Structure of taxol and *trans*-cyclooctene-modified taxol (TCO-taxol). b) Comparison of the ability of 10 μ M taxol, *trans*-cyclooctene taxol, and a DMSO control to polymerize tubulin in the absence of GTP (polymerization assayed through absorbance at 350 nm). Note that *trans*-cyclooctene taxol promotes polymerization similar to taxol and significantly better than a DMSO control. c) Microtubule bundles formed in the presence of *trans*-cyclooctene taxol treated with tetrazine-BODIPY FL (**28**) and visualized by fluorescence microscopy. [Reprinted with permission from Ref. 106 Copyright: John Wiley and Sons]

There is an alternative quenching mechanism called through-bond-energy-transfer (TBET). Unlike traditional FRET, TBET quenching does not require overlapping emission and absorption bands of fluorophores and tetrazines, respectively. In TBET frameworks the fluorophore and the quencher are linked together with a twisted, but otherwise conjugated linker.[114,115] Weissleder and Hilderbrand have studied a set of fluorophore-tetrazine TBET (Figure 22, **32**, **33**) scaffolds to evaluate their fluorogenic nature.[116] Experimental results showed that the orientation of the emission and absorption transition dipoles of the fluorophore and the tetrazine, respectively together with their orientation with respect to the linker that governs the efficiency of TBET quenching. In their particular examples they found the highest EF (900-1600-fold, water) when the fluorescent core and the quenching tetrazine were in meta-position on the benzene ring. This was in good accordance with theoretical predictions. The excellent fluorogenicity was further proven in bioimaging studies using TCO-tagged extra- and intracellular targets. The remarkable EF values allowed imaging with outstanding sensitivity and very low background signal without washing steps.

Prompted by this idea the Wombacher group accounted on the synthesis of rigid BODIPY- and fluorescein-tetrazines (**34**, **35**).[117] These probes allowed excitation in the visible region (λ_{exc} 494-505, λ_{em} 515-524 nm, phosphate buffer pH 7.2) but moderate EF values (4.5-23.4-fold Φ_F enhancements). Their suitability in imaging applications was shown in fluorogenic labeling of TCO modified dihydrofolate reductase. Another set of tetrazine-BODIPY (**36**) [118] and xanthane dyes (**37**, **38**) [119] was introduced by Devaraj and co-workers (Figure 22). The BODIPY probes were specifically developed to detect DNA and microRNA templates in picomolar concentrations. Most recently, Weissleder and co-workers constructed a series of coumarin-tetrazine TBET probes (**39**) that showed outstanding EF values (Figure 22).[120] Fluorescence of the coumarin cores were efficiently quenched by tetrazines and restored upon reaction with TCOs. Though the excitation wavelengths were in the less favorable far UV region (λ_{exc} 347-400, λ_{em} 455-502, PBS pH 7.4) changes in Φ_F justified to call these probes as “HELIOS-probes” for their HypEmissive Ligation-Initiated Orthogonal Sensing capabilities. Upon reaction with TCO 2500-11,000-fold increase in quantum yields were observed. The authors chose epidermal growth factor receptor (EGFR) on the surface of cancer cells as a model system to test the performance of these probes. Images were generated within seconds and exhibited virtually zero nonspecific signal according to the control experiments. Moreover, intracellular imaging of mitochondria and actin network was also accomplished to show the intracellular applicability of these dyes (Figure 23).

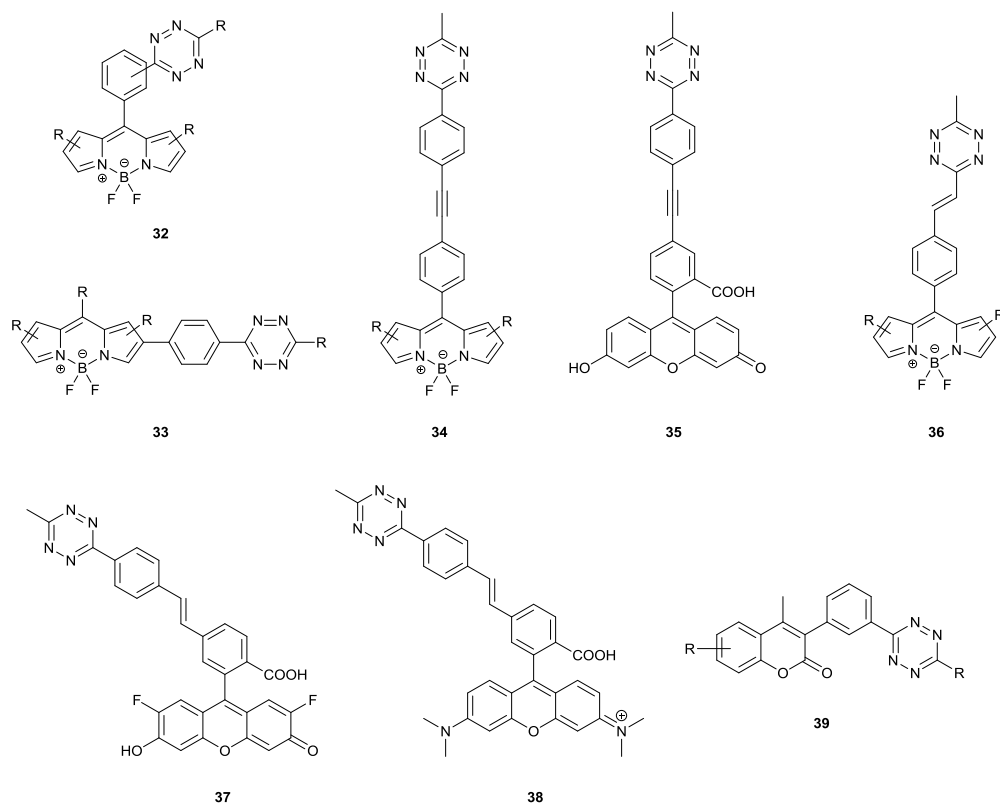


Figure 22. TBET-based tetrazine quenched fluorogenic BODIPY (**32**, **33**, **34**, **36**), xanthene (**35**, **37**, **38**) and coumarin (**39**) dyes with rigid linkers.

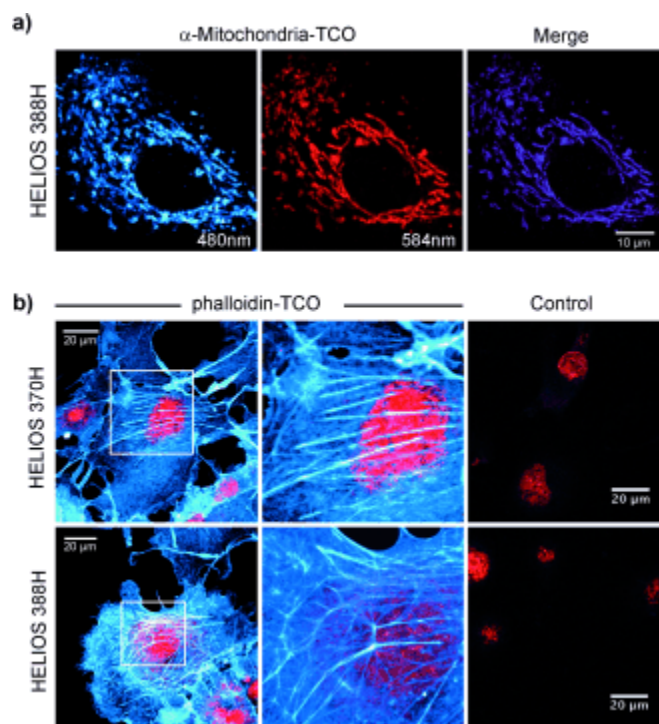


Figure 23. No-wash fluorogenic imaging of intracellular targets. a) Mitochondrial imaging: OVCA-429 cells with RFP-tagged mitochondria were incubated with an anti-mitochondria-TCO antibody, rinsed briefly, and then imaged after addition of 100 nM HELIOS 388H in PBS. Colocalization analysis in ImageJ (Costes auto-threshold) was used to generate the merged image in the right-hand panel (scale

bar=10 μm). b) Actin imaging: COS-1 cells were incubated with phalloidin–TCO (1 $\mu\text{g mL}^{-1}$) and DRAQ5 nuclear counterstain (1 μM , BioStatus), rinsed briefly, and then imaged upon addition of the indicated HELIOS probe at 100 nM. Control images were collected at matched dye concentrations in the absence of phalloidin–TCO (scale bars=20 μm). [Reprinted with permission from Ref. 120 Copyright: John Wiley and Sons]

3.2.6. Other fluorogenic tagging schemes

Although bioorthogonal postulates suggest the use of non-endogenous functions to ensure orthogonal transformations in the presence of a vast number of naturally occurring functions there are few exceptions to these rules. Non-natural arrangement of natural functions can also be used in bioorthogonal tagging schemes. The best examples for this approach are genetically encoded small proteins or peptide tags with unique enzymatic functions (e.g. HaloTag, SNAP-Tag etc.) or tetra-cysteine (Cys₄) self-labeling tags, respectively. Within the context of this review only the latter group will be discussed.

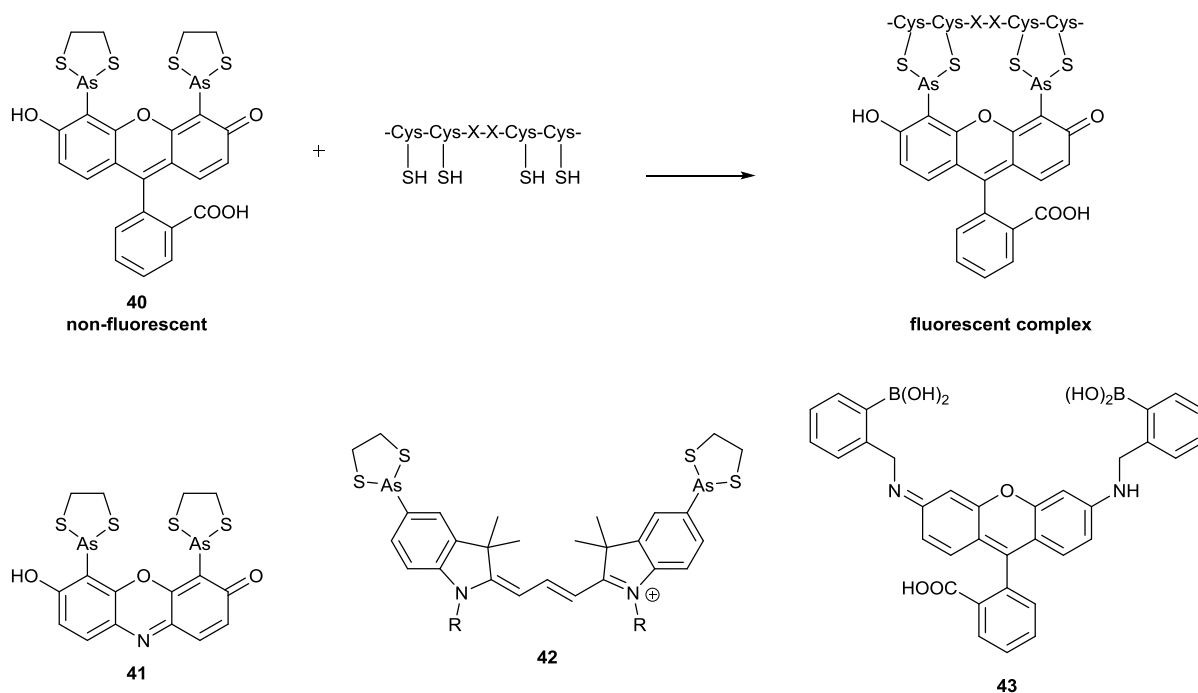


Figure 24. Fluorogenic biarsenical probes and its complex with tetracysteine-containing peptide or protein domain.

Tsien and colleagues introduced the concept by the development of fluorogenic biarsenical probes. Although the initial helix model was revised to be a hairpin structure,[121] the most renowned biarsenical probe is still dubbed as Fluorescein Arsenical Helix binder (F_lA_sH) (Figure 24, 40) referring to the original binding structure. F_lA_sH was able to selectively react with a short 15 amino acid polypeptide tag containing a tetracysteine motif (CCXXCC).[122] Vibrational deactivation or PET by the As-1,2-ethanedithiol groups are supposed to be

responsible for the quenched state of the FAsH probe. Reaction with target Cys₄ tags creates a more constrained structure, which prevents conjugation of the arsenic lone pair electrons with the molecular orbitals of fluorescein. The attained fluorescence enhancement is about 1000-fold (λ_{exc} 508, λ_{em} 528 nm) in aqueous media. The resulting FAsH-peptide conjugate was found to be stable for weeks even in the presence of excess EtSH. Moreover, the FAsH probe is cell permeable and allowed intracellular imaging of HeLa cells expressing a recombinant CFP. The authors later applied FRET technology to image the cytosol and nuclei of HeLa cells expressing mutant calmodulin. Later, the same group developed further biarsenical reagents with different cores (e.g. resorufinol, ReAsH, **41**), which show red-shifted emission (λ_{exc} 593, λ_{em} 608 nm) relative to FAsH.[123] Limitations of these biarsenical probes are the potential toxicity of the arsenic and the competing interaction with non-specific thiols leading to considerable background fluorescence. The need for reducing agents such as DTT or TCEP to prevent the oxidation of SH-groups further limit their use, not to mention that self-labeling peptide tag installation is restricted mostly to the N- or C-termini of the protein of interest with very few examples for internal protein labeling.[124]

The quenching effect of biarsenic motif was applied by Mayer and co-workers in a cyanine biarsenical dye (AsCy3, **42**). They found moderate, 6-fold enhancement (λ_{exc} 560, λ_{em} 576 nm) in aqueous media.[125] It should be noted that AsCy3 was transformed into a membrane-permeable dye suitable for super-resolution imaging.[126] Most recently, Schepartz and co-workers studied the peptide length dependence of an AsCy3 based fluorogenic dye.[127] They found that at least 8 amino acids are needed between the Cys-Cys pairs to reach maximum affinity towards target Cys₄ motif and suppress side reaction with non-specific thiols. They, however, only reached a 3.2-fold increase in fluorescence (with 11 amino acids) upon specific binding. Similar to biarsenicals, bis-boronic acid based fluorogenic labels (RhoBo, **43**) are useful in specific labeling schemes by targeting tetraserine motifs.[128] The specificity of RhoBo was tested on saccharide-rich (HeLa) cell surfaces to image tetraserine-tagged proteins in the cytosol.

Keillor and co-workers took advantage of the quenching effects of a dimaleimide scaffold to design fluorogenic probes. Examples for this setup are naphthalimide (**44**),[129] dansyl (**45**),[130] or coumarin (**46-48**),[131] based bis-maleimides (Figure 25). The PET process accused with the quenching phenomenon allows 7-350-fold enhancement upon Michael addition with Cys₂ motifs. The authors engineered a short alpha-helix sequence (dC10 α (Cys-AA10-Cys) that can be fused to protein of interest.[130]

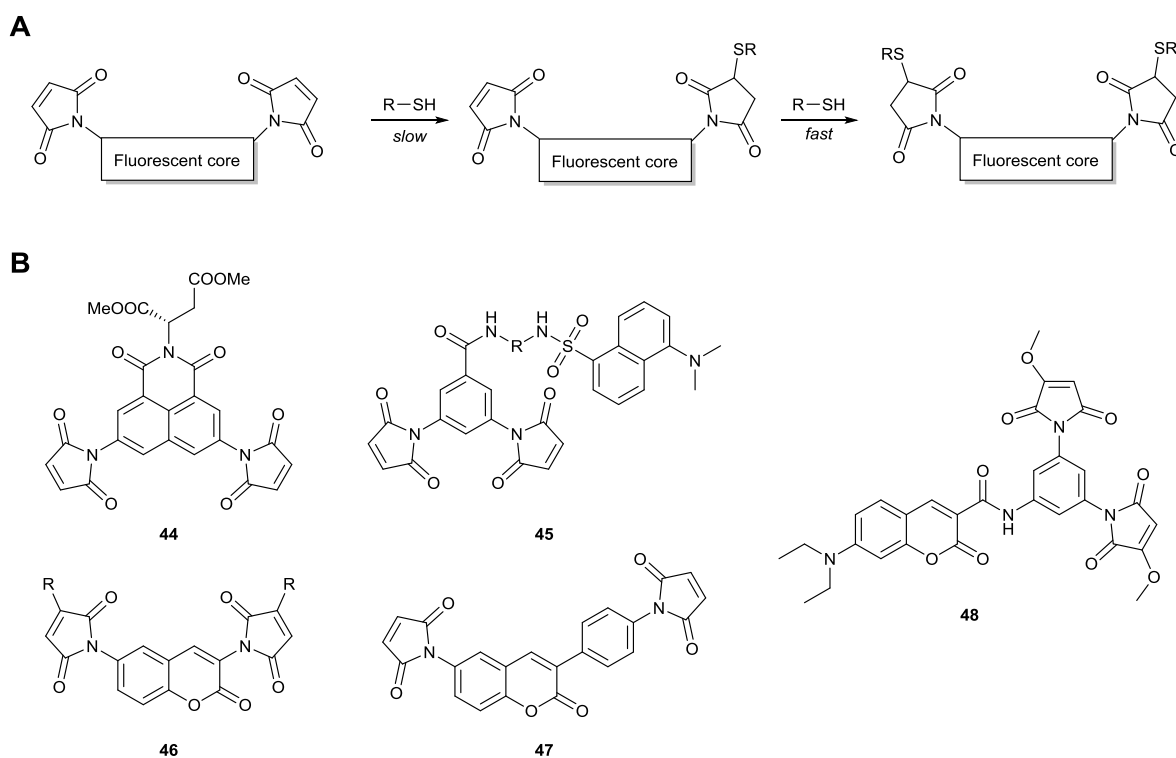


Figure 25. Fluorogenic bis-maleimide probes. A: The general reaction scheme of the double thiol addition. B: 1,8-naphthalimide (**44**), dansyl (**45**) and coumarin (**46-48**) fluorogenics quenched by two maleimide groups.

They found that dimethoxymaleimide probes with attenuated electrophilicity reacted quite specific with target bis-thiols and their reaction with non-specific biothiols (GSH) was completely suppressed. The good membrane permeability of these bis-maleimides was demonstrated in the intracellular labelling studies of recombinant histone H2B-dC10 α , and dC10 α -actin. These tagged proteins were successfully tagged and imaged in the cytosol and nuclei of HEK293T cells using fluorescence microscopy, without any washing steps.[130]

3.3. Bioorthogonalized luminescent nanocomposites

With the development of bioorthogonal chemistries nanocomposites benefited significantly in terms of conjugation capabilities. Owing to their unique properties, nanomaterials are attractive targets for bioconjugation.[132] Besides their genuine attributes such as being protective nanocarriers with high cargo capacity of e.g. drugs with high load capacities and potential for controlled release, many nanocrystalline material exhibit remarkable physical properties.[54,132] Among these features, nanoparticles with the potential for light emission are the most relevant to this review.[54] From the photochemical point of view it can generally be stated that NPs being either intrinsically luminescent or due to dopants exhibit bright photoluminescence with quantum yields close to unity and their photostability is

far better than those of small synthetic dyes. It should also be mentioned that most NPs are not toxic and do not suffer from non-specific binding to e.g. cellular proteins.[54,132]

Nanoparticles have their characteristic intrinsic properties, however, it is usually necessary for biological applications that they are covered with a translucent shell that on the one hand does not affect luminescent properties and on the other hand can be further functionalized e.g. with bioorthogonal functions. Bioorthogonal modification schemes offer clean, efficient and controllable derivatization of nanoparticles. There are two main reasons that NPs are rendered bioorthogonal: i) to use them in targeted tagging schemes and ii) to display other elements on their surface (e.g. drugs, other signaling modules or recognition elements) using efficient chemistries resulting in high coverage. The most common nanoparticles are either synthetic colloids composed of metals, alloys, semiconductors, carbon allotropes or (bio)polymers. Within this chapter we cover examples for different bioorthogonalized NPs and their usage in bioimaging applications. Surprisingly, relatively few types of luminescent nanoparticles are reported in the literature in the context of bioorthogonality and bioimaging.

3.3.1. *Semiconductor quantum dots (QDs)*

Quantum dots are nanocrystalline particles with typical size between 2 – 10 nm are composed of semiconducting materials. The emission properties of QDs can be fine-tuned synthetically by varying their size and composition.[133] Their wide UV absorption band and narrow photoluminescent band make them ideal for multi-color imaging applications. These features are accompanied with high QYs and photostability. Besides rendering them multifunctional in order to enable further – bioorthogonal – functionalization, biocompatible coating of QDs is also necessary to diminish their inherent cytotoxicity.[134] As mentioned earlier the use of CuAAC chemistry is not amenable for QDs as their emission properties are heavily affected by the presence of the transition metal. In order to avoid the unwanted effects of the metal copper-free bioorthogonal chemistries are applied.

Texier *et al.* conducted a detailed study to assess the effects of copper on the luminescent properties of quantum dots.[135] They incubated commercially available CdSe/ZnS/PEG₂₀₀₀-NH₂ QDs in the presence of CuSO₄/sodium-ascorbate a standard resource of Cu(I) catalyst in azide-alkyne click reactions. They observed that the presence of copper irreversibly decreased the luminescence of the particles. Thus they have used copper-free azide-alkyne chemistry in future applications. The same amine modified CdSe/ZnS/PEG₂₀₀₀-NH₂ particles were reacted with a NHS activated cyclooctynes derivative. These bioorthogonalized QDs with an average hydrodynamic size of ~10 nm and emission peak at around 552 nm were applied on Chinese

Hamster Ovary (CHO) cells to image their cell surface glycans. Prior to labeling the CHO cells were treated with azido-tagged mannosamine (ManNAz). The cells incorporated the ManNAz into their cell-surface glycan structure via the metabolic salvage pathway. Bioorthogonalized CHO cell surface then was successfully imaged using the QDs harboring the complementary bioorthogonal function (Figure 26).

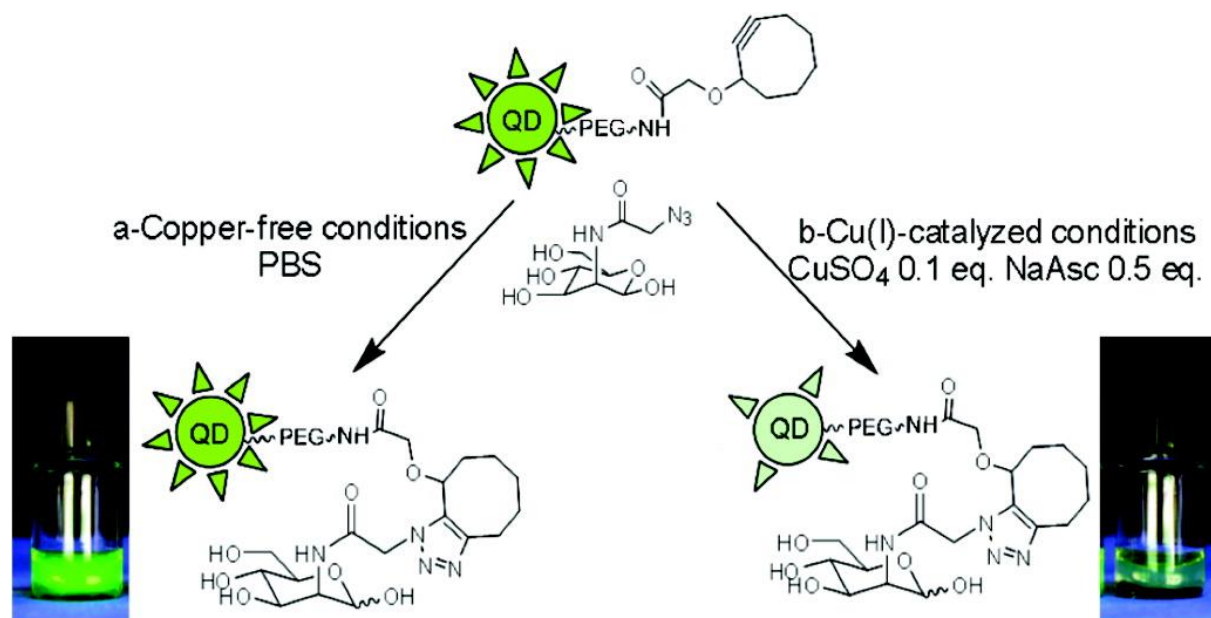


Figure 26. The effect of copper catalyst on the fluorescence properties of “click-functionalized” quantum dots. [Reprinted with permission from Ref. 135 Copyright (2010) American Chemical Society]

In their joint work, the groups of Bawendi and Weissleder devised a biocompatible coating for QDs that was further functionalized with norbornene units to display bioorthogonally applicable moieties on the particles.[136] They have used polymeric imidazole ligands (PILs), random copolymers of poly(ethylene glycol), amino-PEG₁₁ and imidazole, which ensure water solubility, further functionalization and QD-binding, respectively. These PILs were modified with norbornenyl acetic acid succinimide ester via amide bond formation. The as-modified norbornene-PILs (NBPILs) were used to modify the natively capped QDs by ligand exchange. To demonstrate the versatility of this capping method the authors applied a tetrazine-modified Alexa dye on the norbornene decorated QDs to promote inverse electron demand Diels-Alder reaction. According to the molar absorptivities of the Alexa dye and QDs the modification ratio was determined as 16-dye molecule / QD particle, which also represents the number of norbornene units per particle. The developed NBPILs allow high loading of the particles with reactive bioorthogonal motifs while maintaining the neutral charge. In contrast, former amine or carboxylic acid containing coatings resulted in unwanted non-specific binding to cells or biomolecules due to their charge.

In their recent work the same authors aimed at developing QD based luminescent probes for *in vivo* cytometric imaging of rare cells in unmanipulated mice using the same NBPIIL capped QDs.[137] They prepared a diverse combination of norbornene decorated QDs composed of different materials e.g.. CdSe/CdZnS, CdSe/CdS and InAs/CdZnS with emission peaks at around 612, 570 and 800 nm, respectively (QD₆₁₂, QD₅₇₀, QD₈₀₀) and tetrazine modified antibodies (anti-mouse CD31, CD45, c-kit, and Sca-1). They have studied the hydrodynamic size of the Ab conjugated QDs as this parameter influences a lot of biologically relevant parameters such as accessibility, distribution and clearance not to mention the motion of the targeted species. Since NBPIILs coordinate directly to the surface of the particles via their imidazole units smaller hydrodynamic size can be achieved compared to e.g. commercially available water-soluble QDs covered by amphiphilic polymers. In this experiment the average hydrodynamic size around the ~5.8 nm inorganic cores was ~15 nm (for QD₆₁₂). The NBPIIL modified QD-antibody conjugates possessed moderately negative surfaces as indicated by zeta-potential measurements. Compared to commercially available hydrophilic QDs the hydrodynamic size of NBPIIL-covered QDs did not change after incubation in serum indicating minimal non-specific binding of proteins. With these QD immunoconstruct *in vivo* single cell labeling of rare populations of hematopoietic and progenitor cells was successfully achieved and visualization of targeted cells in their native environment in live animals became possible. Moreover, the applied multiphoton microscopy enabled deeper tissue penetration and lower autofluorescence (Figure 27).

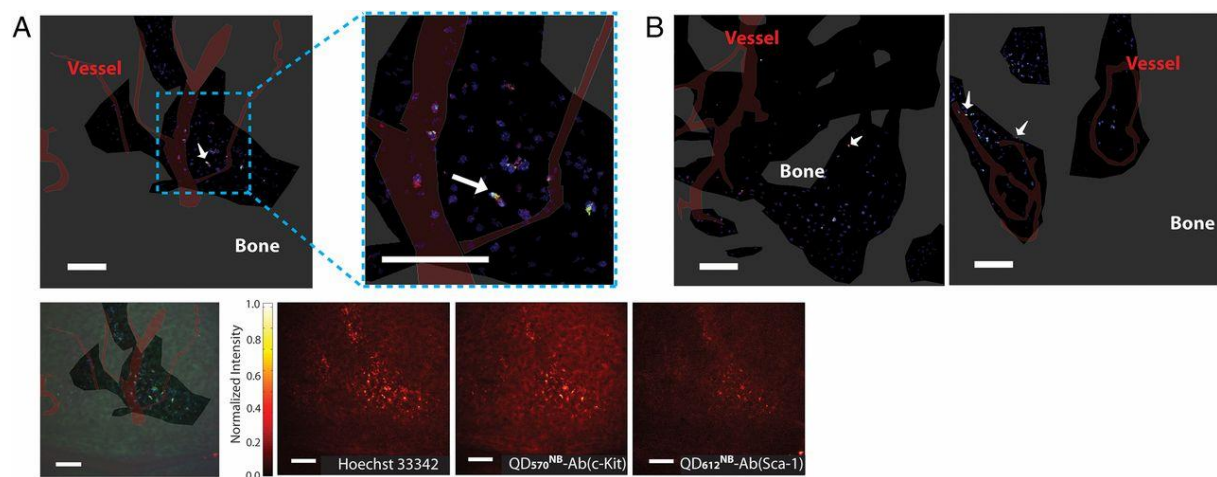


Figure 27. *In vivo* imaging of single endogenous Sca-1⁺c-Kit⁺ cells in the intact bone marrow using QD^{NB}-TzAb. (A, Upper) A representative multiphoton microscopy image of a bone marrow cavity shown after removing the signal from the QD/Ab channels outside of the cells, which were segmented from Hoechst 33342 signal. Yellow cells (arrows) represent single Sca-1⁺c-Kit⁺ cells. Red and green cells represent Sca-1⁺ and c-Kit⁺ cells, respectively. An area containing an Sca-1⁺c-Kit⁺ cell is magnified in Upper Right. Translucent red and gray areas represent vessels and the bone, respectively. Lower Left shows the unmodified maximum intensity projection (~10 μm in the z direction). Lower Right shows

the maximum intensity projections of each channel individually. (B) Additional images of bone marrow cavities containing Sca-1⁺c-Kit⁺ cells. Signals outside of the Hoechst 33342⁺ cells were discarded in these images, e.g., in A, *Upper*. (Scale bars: 100 μm . [Reprinted with permission from Ref. 137 Copyright (2015) National Academy of Sciences, USA.]

In another recent contribution by the Ma and Cai groups the noninvasive visualization of viral infection was accomplished by bioorthogonalized quantum dots.[138] In their report they used CdSeTe/ZnS quantum dots that were coated with azide-modified multidentate polymeric ligands bearing imidazole as coordinating group. These azide functionalized NIR emitting ($\lambda_{\text{em}} = 750 \text{ nm}$) particles with a hydrodynamic diameter of $\sim 13 \text{ nm}$ were conjugated to cyclooctynes derivatized avian influenza H5N1 pseudotype (H5N1p) viruses via strain promoted azide-alkyne cycloaddition to afford luminescent virus constructs (QD-H5N1p). The infectivity of the NIR emitting viruses were found to be unaffected by the QD modification. Mice infected intranasally with live or heat inactivated QD-H5N1p constructs and imaged through the NIR channel. In case of active viruses a bright and sustained fluorescent signal was observed in the lungs, while inactivated viruses displayed distinctly decreased signal. The same active QD-H5N1 construct was used to test the effects of anti-viral drugs (Figure 28). Drug treatment resulted in decrease of signal accumulation in lungs indicating the effects of antiviral treatment. Such bioorthogonally modified systems therefore are promising applicants for the development of antiviral drug screening systems.

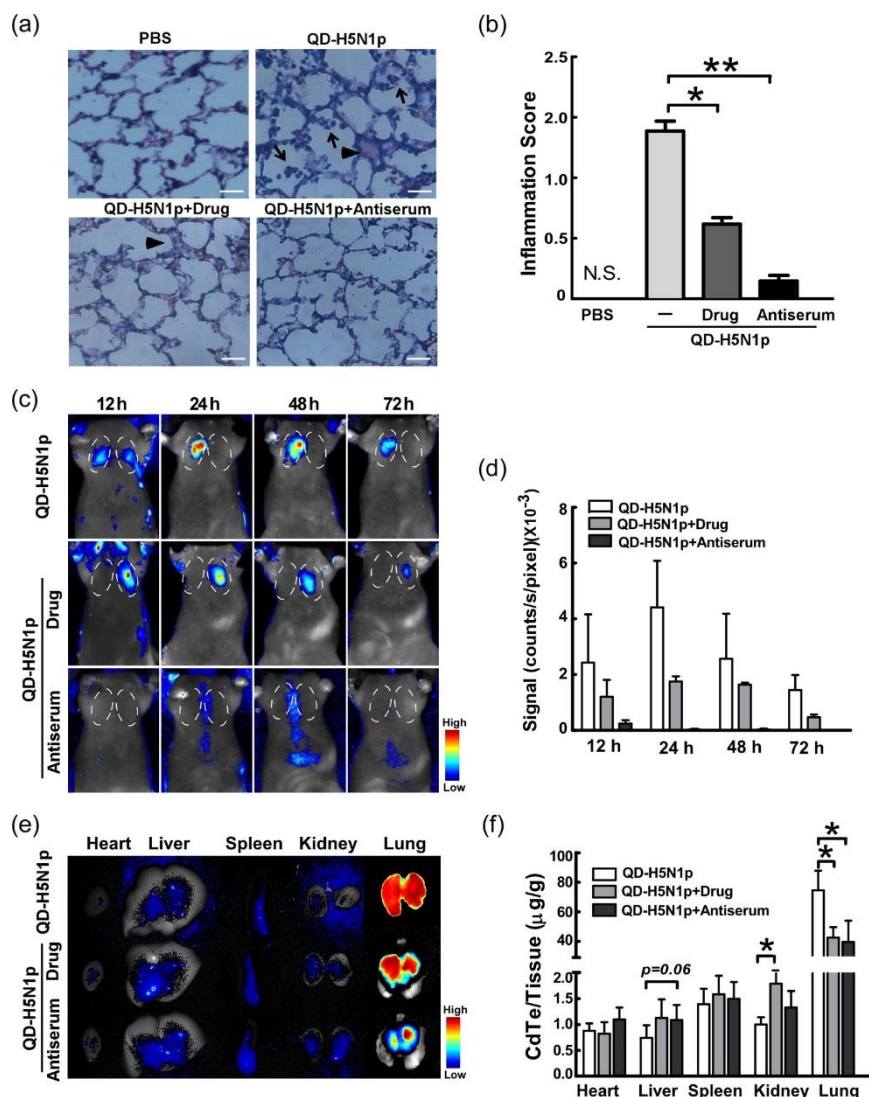


Figure 28. Effect of antiviral agents on the dynamics of respiratory QD-H5N1p infection in mice. Six week old female Balb/c mice were i.n. infected by PBS or QD-H5N1p \pm oseltamivir carboxylate (drug) or mouse antiserum against H5N1p (antiserum). (a,b) Histopathology of lung tissues on day 3 post-infection was assessed by the H&E staining (a), followed by histopathology scoring (b). (↑) Infiltrated inflammatory cells; (▲) thickening of lung epithelium. Scale bar = 20 μ m. (c,d) *In vivo* live imaging of mice at 12–72 h post-infection, and the fluorescent signals of circled regions. (e) *Ex vivo* fluorescent imaging of hearts, livers, spleens, kidneys, and lungs on day 3 post-infection. (f) ICP-OES analysis of cadmium concentration in different organs 3 days post-infection. Tissue cadmium concentration (μ g/g) was calculated by normalizing the amount of cadmium to sample weight. Bars shown are mean \pm SE ($n = 5$), and the differences among groups were determined using one-way ANOVA analysis; * $p < 0.05$; ** $p < 0.01$. [Reprinted with permission from Ref. 138 Copyright (2014) American Chemical Society]

3.3.2. Lanthanide doped nanoparticles – upconverting nanoparticles, UCNPs

Lanthanide-doped upconverting nanoparticles (UCNPs) – sometimes termed as upconverting nanophosphors – are capable of converting low energy (near infra-red) light into higher energy, visible light via sequential multi-photon absorption and energy transfer processes.[139,140] Their NIR excitation enable virtually autofluorescence-free imaging techniques with deeper tissue penetration. Moreover, these features are paired with low

cytotoxicity, narrow emission bandwidth, highly photostability and last, but not least, NPs do not blink. Several bioimaging applications harvest the excellent photophysical properties of UCNPs even in challenging biological media such as blood, however, in combination with bioorthogonality surprisingly few records could be obtained.[141] This is somewhat unexpected, as excellent methods exist for the bioorthogonal modification of UCNPs.

A simple, but efficient method for the modification of hexagonal phase NaYF_4 nanoparticles doped with Yb and Er or Tm was reported by Wolfbeis et al. to make these nanophosphors amenable to click chemistry.[142] Similar to other metal-oxide (hydroxide) surfaces UCNPs can easily be coated with silane reagents to form a hydrophobic silica shell around the particles. When tetraethoxyorthosilicate was applied simultaneously with either (3-azidopropyl)triethoxysilane or prop-2-yn-1-yl (3-(triethoxysilyl)propyl)carbamate using a modified Stöber method azide or alkyne decorated silica coated UCNPs were obtained. Such clickable UCNPs were further modified by means of copper catalyzed azide-alkyne cycloaddition with biotin, maleimide or small organic fluorophore derivatives harboring complementary functions providing evidence for the versatility of this straightforward modification method. The groups of Wagenknecht and Wolfbeis gave an account of making highly functionalized DNA-UCNP constructs using similar azide decorated silica coated green (550 nm) and red (660 nm) emitting $\text{NaYF}_4:\text{Yb,Er}$ UCNPs and alkyne modified oligonucleotides.[143] The obtained DNA-UCNP constructs were highly water soluble compared to plain UCNPs. They have tested the recognition abilities of these DNA-UCNPs in the presence of the counterstrand DNA sequence. Thermal dehybridization experiments using UV absorption together with duplex formation in the presence of ethidium-bromide confirmed that the conjugate can recognize its complementary DNA sequence (Figure 29).

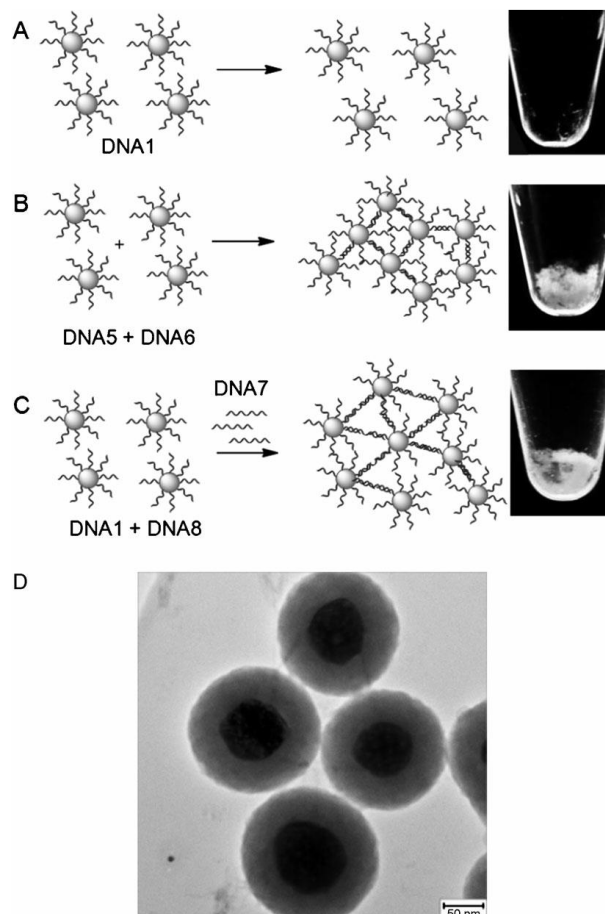


Figure 29. Aggregation of UCNP–DNA conjugates: A) Control with UCNP–DNA1 without cross-linker oligonucleotide. B) UCNP–DNA5+UCNP–DNA6. C) UCNP–DNA1, UCNP–DNA8 and DNA7. D) TEM Image of aggregate B. [Reprinted with permission from Ref. 143 Copyright: John Wiley and Sons]

The imaging applicability of DNA-UCNPs was tested in cells. Normal rat kidney cells were treated with the nanoparticle constructs and imaged using confocal microscopy equipped with an external 980 nm laser source. The cells ingested the particles and upon NIR excitation the upconverted emission colors could be seen without blinking or photobleaching. The authors also investigated the sequence selective aggregation properties of the constructs. When two DNA-UCNP constructs bearing complementary DNA strands were mixed aggregation of the particles could be observed. In a parallel experiments when two particle constructs decorated with non-complementary DNA sequences (**DNA1** and **DNA8**) were mixed no aggregation could be observed. However, aggregation could be initiated when a cross-linker DNA sequence (**DNA7**) complementary with both DNA-UCNP constructs was added. These experiments confirmed that DNA-UCNP conjugates had retained recognition properties and are promising luminescent materials for bioanalytical applications ea. in DNA and RNA recognition applications.

Branda and Baillie introduced an azide coated UCNP system that was further manipulated with alkyne derivatized photoactive dithienylethene (DTE) photoswitchable unit. In their report they used NaYF₄:Yb,Er (20 mol% Yb³⁺, 2 mol% Er³⁺). This UCNP has characteristic emission peaks in the green and the red region (550 and 660 nm, respectively).[144] The original oleic acid capping ligands were replaced by azidopropylphosphonate ligands to afford azide functionalized particles. Copper catalyzed azide-alkyne cycloaddition reaction with an alkyne and PEG bearing DTE afforded DTE-UCNP conjugates. The DTE motif can be reversibly toggled between an open and a closed form using UV and visible light as trigger. UV irradiation induces a photocyclization of the DTE affording a closed DTE that absorbs efficiently the green emission of the UCNP either via energy transfer (FRET) or inner filter mechanism. Irradiation with visible light (< 460 nm) induces a reverse photochemical reaction and leads to ring opening of the DTE. Upon ring opening the intensity of the UCNP green emission reinstates. This photomodulation could be carried out for several photochemical cycles using alternating UV and visible irradiation with minimal changes in the switchability (Figure 30).

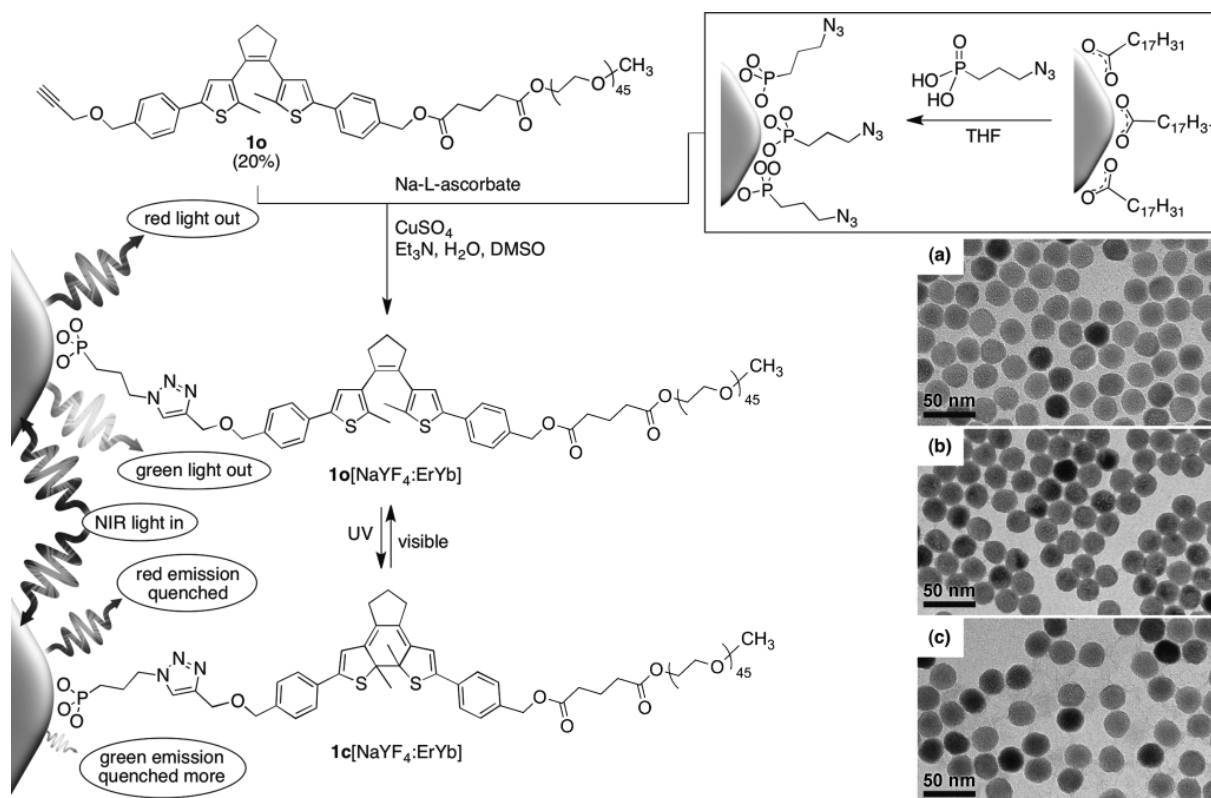


Figure 30. Synthesis of the photoresponsive hybrid system (**1o**[NaYF₄:ErYb]) and a conceptual description of selective quenching of the emission from the nanoparticles by ring-closing the photoswitch. The images are TEM micrographs that show a) the oleate-coated nanoparticle starting material, b) the azide-coated nanoparticles, and c) the nanoparticles decorated with the ring-open form of the photoswitch (**1o**[NaYF₄:ErYb]); this illustrates the uniform size and shape. [Reprinted with permission from Ref. 144 Copyright: John Wiley and Sons]

The UCNP-DTE conjugate was successfully tested in nematodes as well. Moreover, no toxicity or sensitivity towards the constructs could be observed. Such photomodulated UCNPs have the advantage over caged fluorophores as their luminescence can be repeatedly cycled between the two states. Thus, these constructs are promising tools in super-resolution microscopy applications.

An elegant and smart approach for the functionalization of UCNPs was introduced by Haupt and Bui.[145] They took advantage of the nanolamp properties of UCNPs. In their respective work they used diversely functionalized (epoxyde, alkyne, benzamidine or carboxylic acid) acrylic acid derivatives as photopolymerizable monomers. Their method relied on the light emitted by the particles upon NIR excitation. In the presence of a photosensitizer the produced visible light induced photopolymerization of the monomeric species. Since the emission of the particles is weak the polymerization is confined to the close proximity of the particles resulting in the formation of a fine shell around the particles.

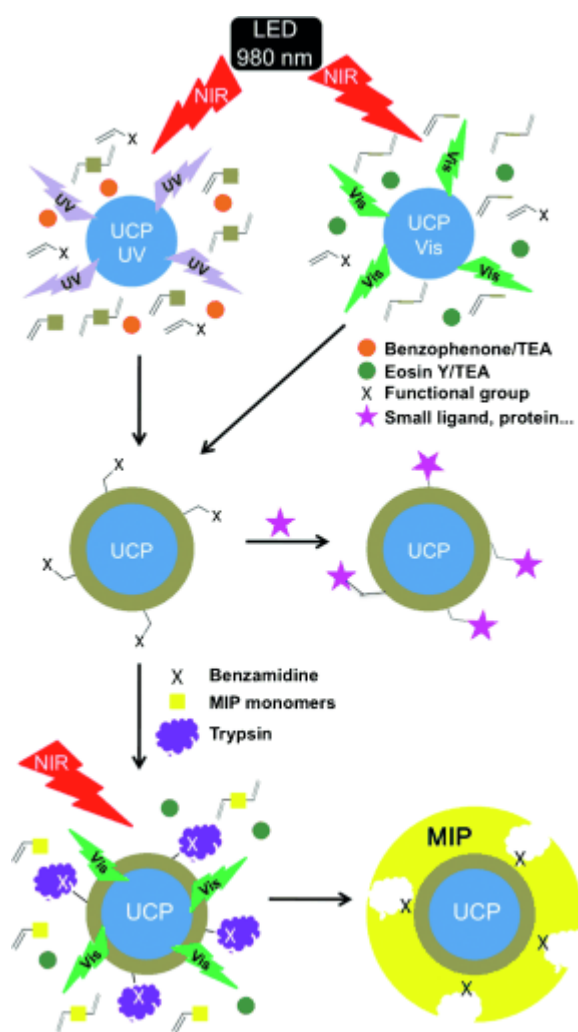


Figure 31. UV or visible light emitted from upconverting nanoparticles excited in the near-infrared region (980 nm) is used to create a polymeric shell in situ around the particles by photopolymerization. Benzophenone and eosin Y are used as UV and visible initiators, respectively. The incorporation of functional monomers enables the subsequent attachment of small ligands, proteins, or other moieties. A second shell, for example, a molecularly imprinted polymer (MIP), can be synthesized by re-initiation in the presence of different monomers and a molecular template (trypsin). LED=light-emitting diode. [Reprinted with permission from Ref. 145 Copyright: John Wiley and Sons]

The authors used two different UCNPs, a visible light emitter NaYF₄:Yb,Er (UCNP-Vis) and a UV emitter Na_{0.6}K_{0.4}YF₄:Yb,Tm (UCNP-UV). They have tested the two UCNPs in the presence of different sensitizers and found that UCNP-Vis/eosine and UCNP-UV/benzophenone systems are ideal for shell formation processes (Figure 31). The shell thickness was dependent on the time allowed for polymerization, the concentration of monomers and sensitizers. Further modification of the core-shell particles was achieved using the functions incorporated through the polymerization process. For example, FITC-N₃ was used to fluorescently label the alkyne coated particles via CuAAC. The platform can also serve as a basis of a second shell e.g. in the construction of molecularly imprinted polymers.

3.3.3. Carbon allotropes, fluorescent nanodiamonds, FNDs

Several nanosized carbon allotrope particle exist, however, herein we restrict our attention to a recently emerged allotrope, namely fluorescent nanodiamonds (FNDs) for their excellent luminescent properties and promising future applications.

Fluorescent nanodiamonds are luminescent, biocompatible nanoparticles between five and several hundred nanometers.[146,147] Their visible excitation results in a NIR emission band centered at around 700 nm. Their emission that originates from nitrogen-vacancy centers is completely resistant to photobleaching or blinking, which allows their use in techniques (e.g. SRM) where large laser power is required. To enhance their dispersibility in water and to reduce their non-specific binding to proteins or to install further surface modification abilities, surface of FNDs needs to be modified as in the case of many other nanoparticulate systems. Cigler and co-workers reported on the development of a “translucent” shell around FNPs that leaves the photophysical characteristics of the nanodiamonds unaffected.[148,149] They utilized a modified Stöber method to form a thin silica shell using TEOS and 3-(trimetoxysilyl)propyl methacrylate. The terminal methacrylates served as a polymerizable platform that afforded “grafting from” coating for further functionalization. In their study they used poly[N-(2-hydroxypropyl)methacrylamide] (poly(HPMA)) with a small amount of propargylacrylamide or 3-(azidopropyl)methacrylamide to afford a hydrophilic biocompatible coated FNDs ready for click conjugation that was resistant to protein adsorption. With this method they formed a 2-5 nm thick shell around the nanoparticles. The alkyne modified FNDs were further modified with several azide-derivatized compounds e.g. fluorogenic coumaryl-azide (Figure 10, **1**) or a radiolabeled GGGRGDSGGGY-azide (RGD-azide) a vectoring molecule for tumor cell targeting. In a following work the same group has used a modified version of this robust method to construct a luminescent platform to image human prostate cancer cells. In this latter

contribution the FNDs (**ND1**) were first coated with a thin silica shell using TEOS (**ND2**). This step was followed by shell growth using (3-aminopropyl)triethoxysilane (APTES) that enables further modification and crosslinking-agent bis(triethoxysilyl)ethane to improve the shell's resistance to hydrolysis (**ND3**). The amino-functionalized nanodiamonds were then modified with heterobifunctional PEG bearing N-hydroxysuccinimidyl and alkyne moieties (**ND4**). Finally, RGD-azide was installed via CuAAC chemistry to afford RGD bearing FNDs (**ND5**). In contrast to naked FNDs, coated nanodiamonds were found to be stable in *in vitro* tissue culture proteins.[147]

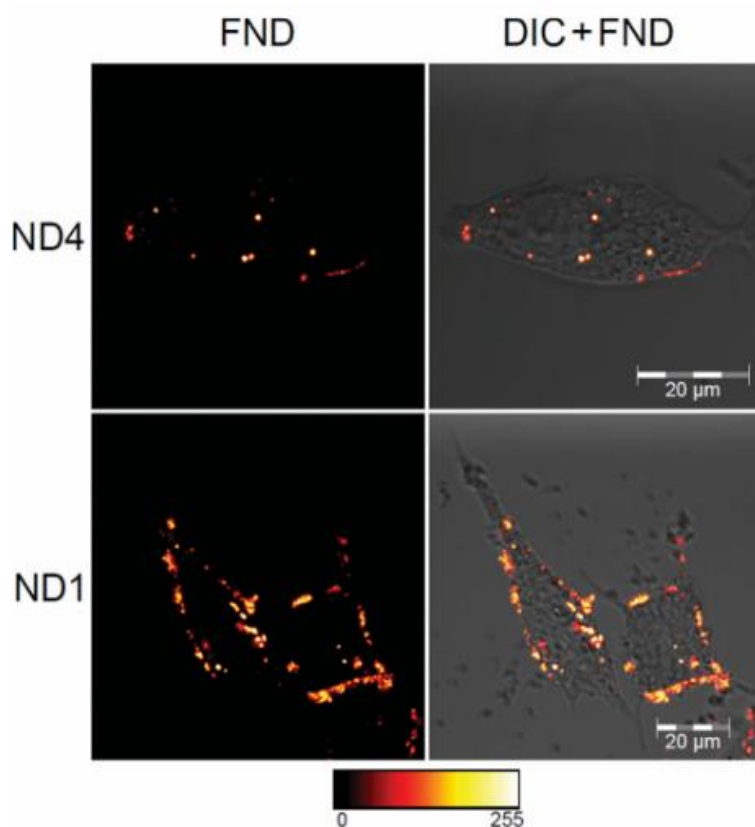


Figure 32. Confocal microscopy images of PEGylated aminosilica- coated (**ND4**) and noncoated (**ND1**) particles preincubated in PBS and internalized by LNCaP cells. The displayed images are fluorescence from NDs (FND) in false colors (left) and merged differential interference contrast (DIC) and FND fluorescence (right). FNDs were dispersed in PBS before adding to cells in medium (final concentration $200 \mu\text{g ml}^{-1}$). Cell were washed by PBS after one hour incubation, incubated for subsequent 23 hours and observed after fixation. Fluorescence of FND was collected by Zeiss LSM 780 at 639–758 nm upon excitation at 532 nm. [Reprinted with permission from Ref. 148 Copyright: John Wiley and Sons]

The authors examined the differences between naked (**ND1**) and coated (**ND4**) nanoparticles in interaction with human prostate cancer cells. The particles were internalized without non-specific cell-membrane adhesion. The naked FNDs however, showed much greater non-specific affinity for cell surfaces, and aggregated inside cells (Figure 32). At the same time the

colloidal behavior of **ND4** particles was not affected providing evidence that such FND-constructs are versatile platforms for imaging studies.

3.3.4. *Doped SiNPs*

Silica is a biocompatible and versatile material that can be readily modified with diverse chemical functions, including bioorthogonal moieties. As seen above, silica shell is often formed around inorganic NPs as a biocompatible shell. The size of silica nanoparticles that are most often formed using the Stöber method ranges between tens and hundred nanometers. SiNPs has the unique feature that they can be doped with a wide range of materials.[150] For example, SiNPs can host 10^4 fluorescent organic dye molecules within 50-75 nm particles. Besides, the silica matrix enhances the photostability and the brightness of dopant organic dyes. Even a defined composition of different dyes can be doped at different concentrations so that can be fabricated to construct color-“barcoded” labels.

A method, suitable for the multiple functionalization of SiNPs was introduced by the Lin group.[151] Their silica platform was suited to incorporate fluorescent dyes, targeting moieties to recognize certain cancer cell-lines, and an anti-cancer drug. They have started their synthesis by forming 40 nm plain silica nanoparticles (**HO@SiO₂NP**) by means of conventional Stöber method. Next a fluorescent shell was formed around these particles using APTES and Cy3-silane in a 100 to 1 ratio to afford amino-functionalized Cy3-doped NPs (**NH₂@Cy3SiO₂NP**). Next an amino-appending di-alkyne, built on a lysine framework was incorporated using conventional activated ester coupling (**di-alkyne@Cy3SiO₂NP**). The di-alkyne moiety included a cyclooctyne and a terminal alkyne function that allows orthogonal stepwise modification by means of sequential SPAAC and CuAAC chemistries, a concept introduced by Wolbeis and Kele.[152,153] The di-alkynylated NPs were then allowed to react with antitumor drug Paclitaxel-azide (PTX) using SPAAC, then with targeting ligand triantennary galactose-azide (TGal) in a CuAAC reaction to afford (**TGal-PTX@Cy3SiO₂NP**).

Stepwise Orthogonal Click Chemistry

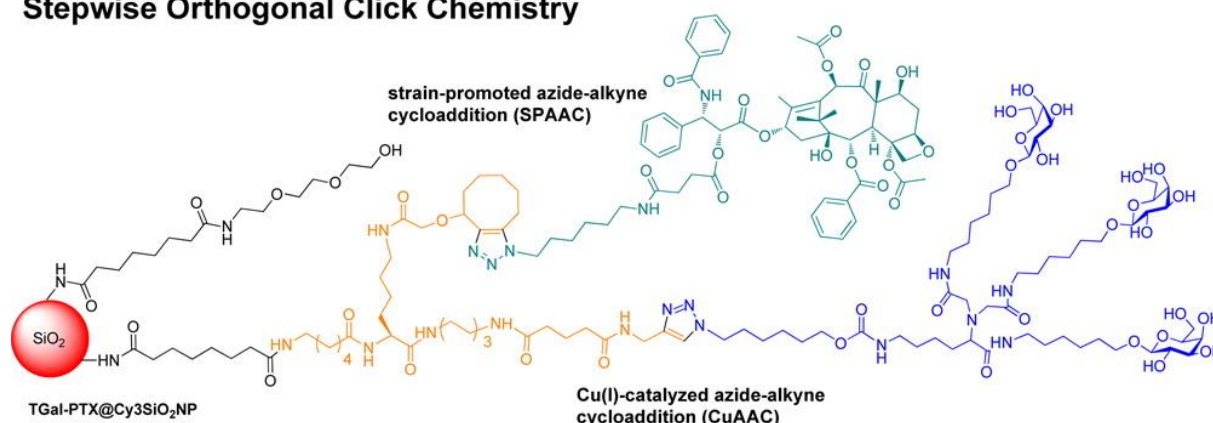


Figure 33. Schematic representation of trifunctionalized SiNPs. [Reprinted with permission from Ref. 151 Copyright (2013) American Chemical Society]

The resulting particles were efficiently functionalized suggesting that the applied bioorthogonal reactions are robust. The size of the particles were determined to be ca. 50 nm, ideal for NP-mediated cellular internalization. To evaluate the anticancer activity of the NPs HepG2 cells were treated with **TGal-PTX@Cy3SiO₂NP**, **TGal@Cy3SiO₂NP** and free PTX. The tubulin network of cells was visualized using DyLight 649-IgG to give purple color. The red color originates from the Cy3 dopants. LysoTracker Green DNS-26 was used to stain late endosomes and lysosomes green, while DAPI was used to label the nuclei (blue). Confocal microscopy images showed that PTX (Figure 34, 1b) and **TGal-PTX@Cy3SiO₂NP** (Figure 34, 1c) cells have similar tubulin pattern indicating the microtubule inhibition effects of PTX. By contrast, **TGal@Cy3SiO₂NP** treated cells showed the same uptake of NPs without the effects of PTX (Figure 34, 1d). The yellow color on the merged images (Figure 34, 5c and 5d) originates from co-localization of red and green fluorescence indicating that the NPs accumulate in late endosomes and lysosomes after endocytosis. Further, cell-proliferation studies revealed that the cytotoxicity of **TGal@Cy3SiO₂NPs** is dose dependent. The authors anticipate that the presented di-alkyne platform provides a versatile modification method for future targeted drug delivery applications using nanoparticulate systems.

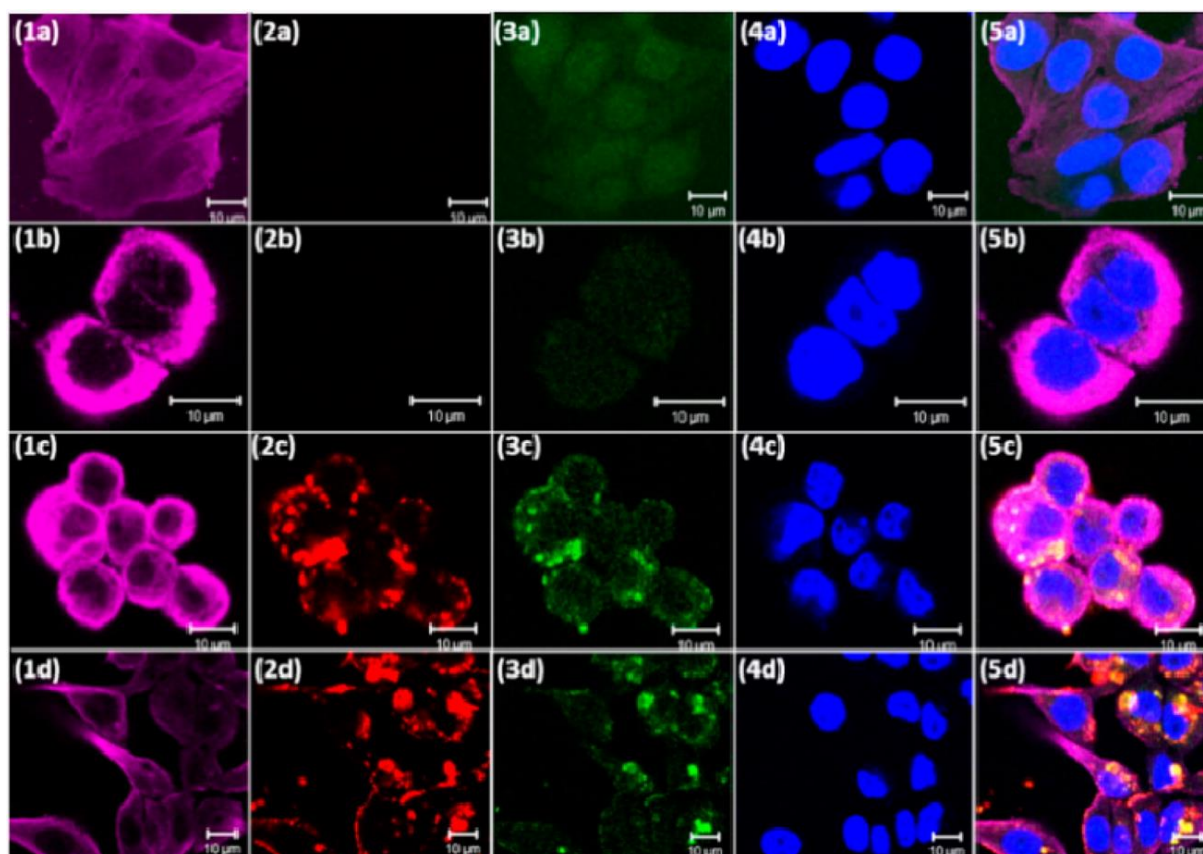


Figure 34. Confocal images of HepG2 cells treated with PTX (5.3 μM in 0.5 mL serum-free DMEM), **TGal-PTX@Cy3SiO₂NP** (100 $\mu\text{g}/\text{mL}$ in 0.5 mL serum-free DMEM), or **TGal@Cy3SiO₂NP** (100 $\mu\text{g}/\text{mL}$ in 0.5 mL serum-free DMEM) for 2 days. Each horizontal row of images (a-d) represents: (a) control without added reagents as control, (b) PTX with 3.3% DMSO as a positive control, (c) **TGal-PTX@Cy3SiO₂NP**, and (d) **TGal@Cy3SiO₂NP** as a negative control. The vertically arranged images (1–5) show: (1) purple color representing tubulin distribution; (2) red fluorescence arising from Cy3 dye on silicon oxide NP; (3) green fluorescence associated with LysoTracker Green DND-26 found within the endosomes and/or lysosomes; (4) cell nuclei stained with DAPI, which fluoresces blue; and (5) a merge of the images. The yellow fluorescence indicates that **TGal-PTX@Cy3SiO₂NP** and **TGal@Cy3SiO₂NP** colocalized with LysoTracker Green DND-26 in late endosomes and/or lysosomes. Scale bar: 10 μm . [Reprinted with permission from Ref. 151 Copyright (2013) American Chemical Society]

3.3.5. Magnetofluorescent nanoparticles, MFNPs

Weissleder and co-workers introduced a concept termed BOND for “bioorthogonal nanoparticle detection”.[154,155] In their study they used magnetofluorescent nanoparticles (MFNPs) as markers allowing dual-channel detection. They started from an amine modified cross-linked iron-oxide (CLIO) magnetic core that was modified with amine reactive cyanine dye (VT680).

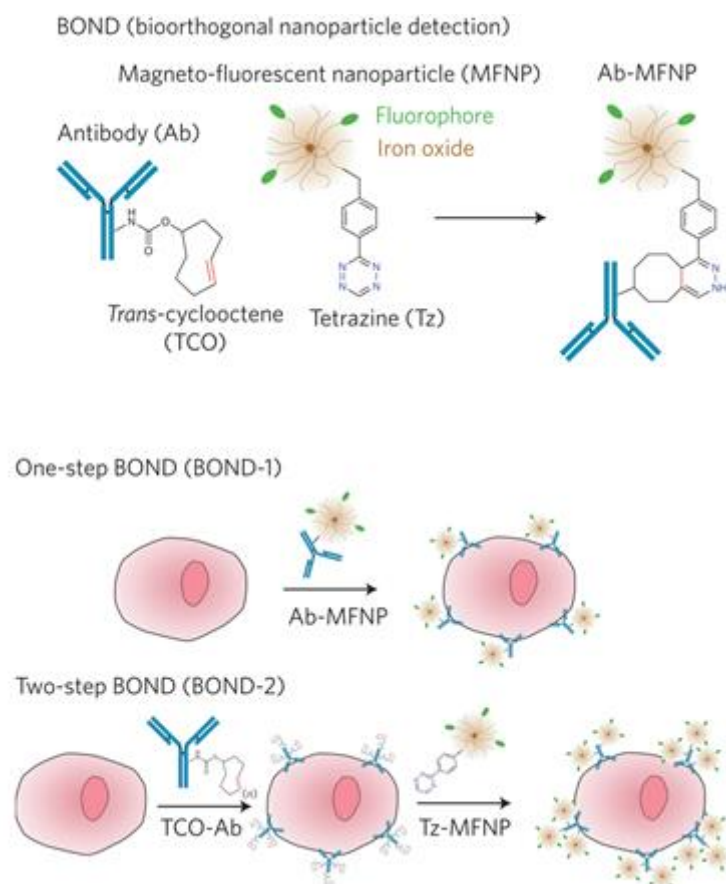


Figure 35. Top: Schematic showing the conjugation chemistry between antibody and nanoparticle. The diagram is a schematic and not to scale. Bottom: Application of BOND for one-step (direct) and two-step targeting of nanoparticles to cells. Note that the antibody and tetrazine are present in multiple copies per nanoparticle (~2–3 antibodies, Ab; 84 tetrazine, Tz). [Reprinted partly from Ref. 154 by permission from Macmillan Publishers Ltd: Nature Nanotechnology, copyright (2010)]

These NP contained approximately 4.7 dye molecules per MFNP and ~84 available primary amine sites. The remaining amines were allowed to react with amine reactive tetrazine (TZ-NHS). Since no primary amine could be detected after the reaction the Tz valency was assumed to be 84 per particle. Parallel to this monoclonal antibody trastuzumab, which is used to clinically treat breast cancers expressing HER2, was modified with trans-cyclooctenes (TCOs) via amide bond formation through the lysine moieties of the antibody. Two methods were tested for targeting extracellular receptors on cancer cells. In one setting the MFNPs were directly modified with the TCO bearing antibodies via inverse electron demand Diels-Alder chemistry (BOND-1). In another setting they used a sequential approach where the cells were first treated with TCO-Abs then with Tz-MFNPs (BOND-2). The authors have explored the performance of BOND-1 and BOND-2 techniques and found that the nanoparticle binding to cells efficiency of BOND-2 was consistently higher by a factor of 10-15 due to binding amplification. This amplification was found to be similar to other two-step schemes, however, the small size of the

bioorthogonal reagents allows for significantly degree of covalent tagging. Using this specific rapid and modular scheme, the same authors accounted on the staining of intracellular biomarkers. Using optimized fixation and permeabilization, the cells were treated with TCO modified anti-cytokeratin (CK) and anti-nuclear protein (K_i-67) antibodies (Figure 36).[156] Subsequent treatment with Tz-MFNPs resulted in specific labelling of the respective proteins. Similarly to previous observations the two-step tagging scheme resulted in amplified signals in contrast to tagging with a directly labeled anti-CK-MFNP conjugate, which may be explained by the much smaller size of TZ-MFNPs (~ 29 nm) relative to immune-conjugates (~ 42 nm).

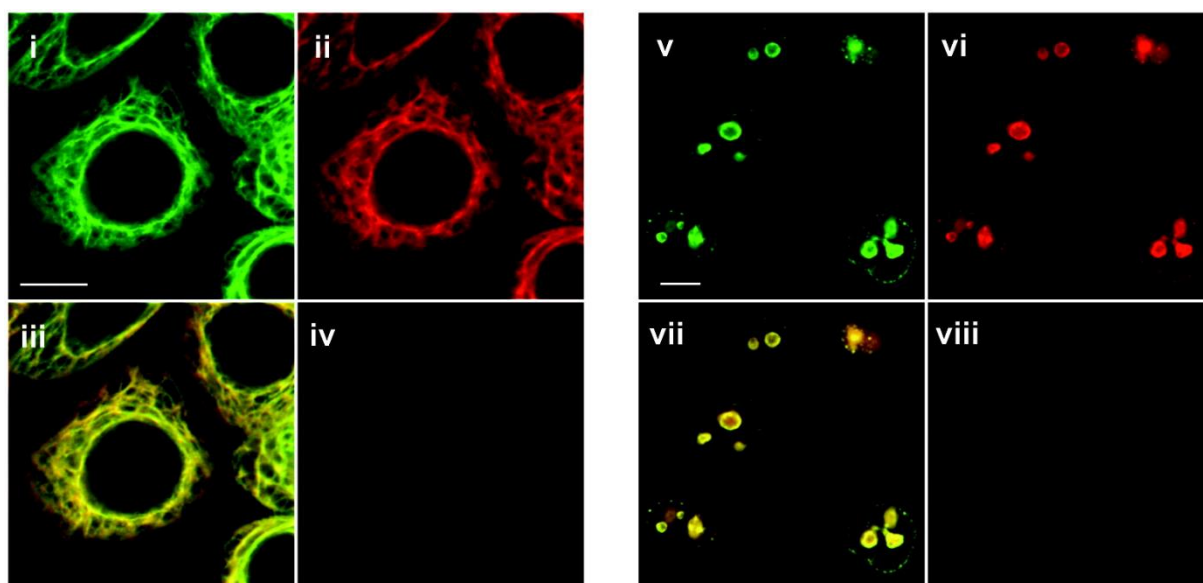


Figure 36. Confocal microscopy images of SK-BR-3 (i–iv) and PANC-1 (v–viii) cells targeted for CK and K_i-67 , respectively. In both cases, antibodies were labeled with both TCO (3–4 per antibody) and AlexaFluor-488 fluorescent dye. Following MFNP labeling, images were captured at 488 (antibody, pseudocolored green, i and v) and 680 (MFNP, pseudocolored red, ii and vi) nm emission. Merged images reveal excellent correlation between the two signals (iii and vii). Controls determined using a nonbinding, TCO-modified control antibody were negative (iv and viii). The scale bars in (i) and (v) represent 10 μm . [Reprinted with permission from Ref. 156 Copyright (2011) American Chemical Society]

Moreover, the dual-channel detection features enabled magnetic resonance imaging of MFNP tagged proteins. Since biological samples exhibit minimal intrinsic magnetic background magnetic detection is possible even in optically obscure samples.

3.3.6. Semiconducting polymer dots (PDots)

PDots are a new class of ultrabright and non-toxic luminescent nanoprobe that consist of *p*-conjugated semiconducting polymeric materials.[157,158,159] They are able to exhibit strong fluorescence, which can be described in terms of semiconductor band theory. For biological

applications, the surface chemistry of the Pdots need to be addressed. Unlike its inorganic counterpart, QDs, the luminescence of Pdots is not affected by the presence of metal ions, thus their use in CuAAC conjugation schemes is obvious. Chiu *et al.* presented a versatile approach, where semiconducting, highly fluorescent poly[(9,9-dioctylfluorenyl-2,7-diyl)-*co*-(1,4-benzo{2,1',3}-thiadiazole)] (**PFBT**) polymer was functionalized with poly(styrene-*co*-maleic anhydride) (**PSMA**).[160] Coprecipitation of **PFBT** and a small amount of **PSMA** resulted in Pdots bear carboxylic groups on their surface, which presents an easily modifiable platform for further conjugations. The Pdots were modified using amino functionalized ethylene glycol azide or alkyne to afford clickable Pdots in the 15 nm size range. These clickable luminescent Pdots were used to image newly synthesized proteins in MCF-7 cells. The cells were metabolically labeled with ManNAz to render surface glycans clickable. Azide-bearing cell-surface glycans were then successfully labeled with alkyne-Pdots using CuAAC chemistry (Figure 37).

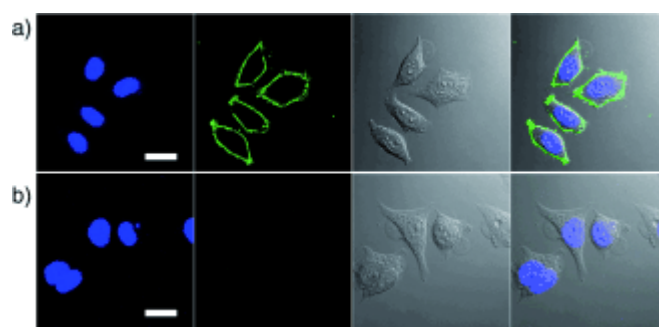


Figure 37. Fluorescence imaging of glycoproteins in GalNAz-treated MCF-7 cells tagged with Pdot-alkyne probes. a) Positive Pdot labeling in the presence of copper(I). b) Negative control for Pdot labeling carried out under identical conditions as in (a) but in the absence of copper(I). The left four panels show fluorescence images; green fluorescence is from Pdots and blue fluorescence is from the nuclear stain Hoechst 34580. The right four panels show Nomarski (DIC) and combined DIC and fluorescence images. Scale bars: 20 μm . [Reprinted with permission from Ref. 160 Copyright: John Wiley and Sons]

3.3.7. Liposomes

Amongst the various methods for the targeted delivery of drugs, liposomes are particularly advantageous.[132,161,162] Besides their enhanced permeability and retention (EPR) effects, coating the surface of liposomes with targeting moieties such as antibodies, proteins, polysaccharides etc. can further increase liposome-based drug accumulation in certain cell-lines.[163] Bioorthogonal chemical approaches are ideal to ensure the correct orientation of such targeting elements. In their account Kim and co-workers has modified PEGylated nanosized liposomes to image azidosialic acid modified cancer cells *in vivo*. [164] 1,2-distearoyl-sn-glycero-3-phosphoethanolamine-N-[amino(polyethylene glycol)₂₀₀₀] (DSPE-

PEG-NH₂) was modified with a dibenzocyclooctyne (DBCO) through amide bond formation (**DBCO-PEG-DSPE**). Parallely, 1,2-dipalmitoyl-sn-glycero-3-phosphoethanolamine (DPPE) was modified with Cy5 by similar means. DBCO-liposomes (**DBCO-lipo**) were synthesized by mixing DPPC : cholesterol : DBCO-PEG-DSPE : Cy5-DPPE in a 54.5: 35: 10: 0.5 molar ratio. The resulting fluorescent nanoparticles were ~75 nm sized, ready for further conjugation via SPAAC chemistry. Xenograft mice models bearing two tumors (A549 tumor) in both sides of the flank region were intratumorally injected with ManNAz at one side. The resulting xenograft models had tumor cells expressing azido-sialates in their surface glycans at one side and normal sialates on the untreated side. Once the tumors reached 10 mm diameter they were given **DBCO-lipo** intravenously. Non-invasive near infra-red imaging of mice showed specific labeling of the azide expressing tumors. In contrast, mice treated with liposomes lacking the cyclooctynes (**PEG-lipo**) showed no difference in fluorescence intensity in the tumors with or without azidosialate (Figure 38). In combination with other orthogonal chemistries installation of other elements (targeting, drug, etc.) is also possible.

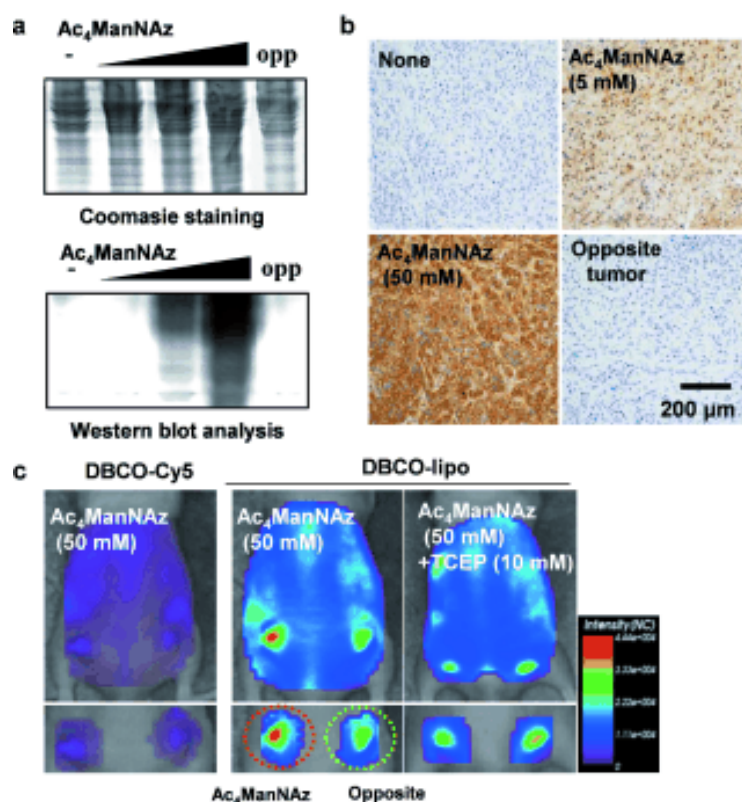


Figure 38. *In vivo* tumor-targeting of DBCO-lipo in tumor-bearing mice models. a) Coomassie staining and western blot analysis of $Ac_4ManNAz$ -treated tumor tissues; opp=opposite (control) tumor. b) Histological staining of $Ac_4ManNAz$ -treated tumor tissues using phosphine-FLAG and FLAG-HRP. c) Whole body biodistribution of DBCO-lipo in $Ac_4ManNAz$ -treated tumor-bearing mice. (left: $Ac_4ManNAz$ -treated, right: saline-treated). [Reprinted with permission from Ref. 164 Copyright: John Wiley and Sons]

4. Summary and outlook

Fluorescent imaging techniques progressed considerably, lately. In the past years we could witness breakage of conceptual and experimental limits in optical microscopy, efforts that were acknowledged by Nobel-prizes in 2008 and 2014. These developments brought us much closer to the understanding of molecular processes inside live organisms. These hardware developments, however, could not have been fully harvested without developments in conjugation techniques. The need for selective installation of signaling units i.e. fluorophores onto biologically relevant targets triggered the exploration of new ways that could be employed even in *in vivo* labeling schemes. Not a surprise then that the last decade has brought considerable progress in the field of covalent conjugation techniques and led to the development of bioorthogonal chemistry.

In vivo fluorescent labeling schemes has probably benefited the most from developments in bioorthogonal ligation reactions. These biocompatible and selective chemical transformations in combination with advanced molecular biology techniques e.g. genetic encoding of non-canonical amino acids allow selective and site-specific fluorescent modulation and subsequent tracking of biologically relevant species. In this review we attempted to give an overview of the state-of-the-art of bioorthogonally applicable fluorescent labels of various kind. These bioorthogonalized fluorescent or fluorogenic small organics or luminescent nanoparticles can be applied to tag selected biological targets harboring the appropriate – complementary – chemical reporter. Although the fluorescent labels listed here are suitable to fulfill the given specific needs, there are many aspects that still could be improved. For example, being orthogonal reactions SPAAC and CuAAC chemistries or certain SPAAC and SPIEDAC reactions allow dual labeling schemes, multicolor imaging schemes require more diverse tagging. For this more development of more orthogonal reactions are required.

Although the existing bioorthogonal reactions would allow selective labeling of intracellular structures most bioorthogonal tagging schemes are employed in the tagging of extracellular targets such as receptors or glycans. For intracellular, specific *in vivo* tagging schemes non-toxic, membrane-permeable, bioorthogonally applicable labels are needed. Furthermore, super-resolution techniques require such probes also to be bright and photostable with minimal background signal. As a consequence, a special attention should be devoted to the development of small, membrane-permeable reagents with bright fluorogenic properties that allow biomolecule- and site-specific labeling of selected structures.

Another promising field in bioorthogonal fluorescent probes is the development of nanoparticulate systems that allow multimodal imaging (e.g. NIR, PET, MRI etc.) that could

also serve as platforms for targeting elements and cargos for drugs at the same time. Design elements of such multi-functionalized nanoparticles also involves the use of multiple orthogonal chemistries for the installation of different modules.

Briefly concluding, existing and newly developed bioorthogonal fluorescent probes can bring us closer to a more comprehensive understanding of living matter. Seeing the whole picture more clearly can help us understand the essence of biomolecular processes and design more efficient drugs e.g. for the treatment of specific tumors.

Acknowledgements

This work was supported by grants from the Hungarian Academy of Sciences (Lendület, LP2013-55/2013) and the Hungarian Scientific Research Fund (NN-110214). The authors wish to thank Mr. Ádám Eördög for the design of the graphical contents. Competing interests: The authors have declared that no competing interests exist.

References

-
- [1] Saxon E, Bertozzi C. R. 2000 Cell Surface Engineering by a Modified Staudinger Reaction *Science* **287** 2007-10
 - [2] Sletten E M and Bertozzi C R 2009 Bioorthogonal chemistry: fishing for selectivity in a sea of functionality *Angew. Chem. Int. Ed. Engl.* **48** 6974-98
 - [3] Patterson D M, Nazarova L A and Prescher J A 2014 Finding the right (bioorthogonal) chemistry *ACS Chem. Biol.* **9** 592-605
 - [4] Sletten E M and Bertozzi C R 2011 From mechanism to mouse: a tale of two bioorthogonal reactions *Acc. Chem. Res.* **44** 666-76
 - [5] Jewett J C and Bertozzi C R 2010 Cu-free click cycloaddition reactions in chemical biology *Chem. Soc. Rev.* **39** 1272-9
 - [6] Chang P V, Prescher J A, Sletten E M, Baskin J M, Miller I A, Agard N J, Lo A and Bertozzi C R 2010 Copper-free click chemistry in living animals *Proc. Natl. Acad. Sci. U.S.A.* **107** 1821-6
 - [7] Ramil C P and Lin Q 2013 Bioorthogonal chemistry: strategies and recent developments *Chem. Commun.* **49** 11007-22
 - [8] Tinnefeld P, Eggeling C and Hell S W 2015 *Far-Field Optical Nanoscopy* (Berlin: Springer)
 - [9] Schilling C I, Jung N, Biskup M, Schepers U and Bräse S 2011 Bioconjugation via azide–Staudinger ligation: an overview *Chem. Soc. Rev.* **40** 4840-71
 - [10] van Berkel S S, van Eldijk M B and van Hest J C M 2011 Staudinger ligation as a method for bioconjugation *Angew. Chem. Int. Ed. Engl.* **50** 8806-27
 - [11] Lin F L, Hoyt H M, van Halbeek H, Bergman R G and Bertozzi C R 2005 Mechanistic Investigation of the Staudinger Ligation *J. Am. Chem. Soc.* **127** 2686-95
 - [12] Yu Z, Ohulchanskyy T Y, An P, Prasad P N and Lin Q 2013 Fluorogenic, two-photon-triggered photoclick chemistry in live mammalian cells *J. Am. Chem. Soc.* **135** 16766-9

-
- [13] An P, Yu Z and Lin Q 2013 Design and synthesis of laser-activatable tetrazoles for a fast and fluorogenic red-emitting 1,3-dipolar cycloaddition reaction *Org. Lett.* **15** 5496-9
- [14] Song W, Wang Y, Qu J, Madden M M and Lin Q 2008 A photoinducible 1,3-dipolar cycloaddition reaction for rapid, selective modification of tetrazole-containing proteins *Angew. Chem. Int. Ed.* **47** 2832-5
- [15] Ramil C P and Lin Q 2014 Photoclick chemistry: a fluorogenic light-triggered *in vivo* ligation reaction *Curr. Opin. Chem. Biol.* **21** 89-95
- [16] Yu Z, Ho L Y, Wang Z and Lin Q 2011 Discovery of new photoactivatable diaryltetrazoles for photoclick chemistry via “scaffold hopping” *Bioorg. Med. Chem. Lett.* **21** 5033-6
- [17] Debets M F, van der Doelen C W J, Rutjes F P J T and van Delft F L 2010 Azide: a unique dipole for metal-free bioorthogonal ligations *ChemBioChem* **11** 1168-84
- [18] Rostovtsev V V, Green L G, Fokin V V and Sharpless K B 2002 A stepwise Huisgen cycloaddition process: copper(I)-catalyzed regioselective “ligation” of azides and terminal alkynes *Angew. Chem. Int. Ed.* **41** 2596-9
- [19] Tornøe C W, Christensen C and Meldal M 2002 Peptidotriazoles on Solid Phase: [1,2,3]-Triazoles by Regiospecific Copper(I)-Catalyzed 1,3-Dipolar Cycloadditions of Terminal Alkynes to Azides *J. Org. Chem.* **67** 3057-64
- [20] Rodionov V O, Presolski S I, Díaz D D, Fokin V V and Finn M G 2007 Ligand-Accelerated Cu-Catalyzed Azide-Alkyne Cycloaddition: A Mechanistic Report *J. Am. Chem. Soc.* **129** 12705-12
- [21] del Amo D S, Wang W, Jiang H, Besanceney C, Yan A C, Levy M, Liu Y, Marlow F L and Wu P 2010 Biocompatible Copper(I) Catalysts for *in Vivo* Imaging of Glycans *J. Am. Chem. Soc.* **132** 16893-9
- [22] Baskin J M, Prescher J A, Laughlin S T, Agard N J, Chang P V, Miller I A, Lo A, Codelli J A and Bertozzi C R 2007 Copper-free click chemistry for dynamic *in vivo* imaging *Proc. Natl. Acad. Sci. U.S.A.* **104** 16793-7
- [23] Debets M F, van Berkel S S, Dommerholt J, Dirks A J, Rutjes F P J T and van Delft F L 2011 Bioconjugation with Strained Alkenes and Alkynes *Acc. Chem. Res.* **44** 805-15
- [24] Jewett J C, Sletten E M and Bertozzi C R 2010 Rapid Cu-Free Click Chemistry with Readily Synthesized Biarylazacyclooctynones *J. Am. Chem. Soc.* **132** 3688-90
- [25] Ning X, Guo J, Wolfert M A and Boons G-J 2008 Visualizing Metabolically Labeled Glycoconjugates of Living Cells by Copper-Free and Fast Huisgen Cycloadditions *Angew. Chem. Int. Ed.* **120** 2285-7
- [26] Debets M F, van Berkel S S, Schoffelen S, Rutjes F P J T, van Hest J C M and van Delft F L 2010 Aza-dibenzocyclooctynes for fast and efficient enzyme PEGylation *via* copper-free (3+2) cycloaddition *Chem. Commun.* **46** 97-99
- [27] Dommerholt J, Schmidt S, Temming R, Hendriks L J A, Rutjes F P J T, van Hest J C M, Lefeber D J, Friedl P and van Delft F L 2010 Readily Accessible Bicyclononynes for Bioorthogonal Labeling and Three-Dimensional Imaging of Living Cells *Angew. Chem. Int. Ed. Engl.* **49** 9422-25
- [28] Varga B R, Kállay M, Hegyi K, Béni S and Kele P 2012 A non-fluorinated monobenzocyclooctyne for rapid copper-free click reactions *Chem. Eur. J.* **18** 822-8
- [29] Knall A-C and Slugovc C 2013 Inverse electron demand Diels-Alder (iEDDA)-initiated conjugation: a (high) potential click chemistry scheme. *Chem. Soc. Rev.* **42** 5131-42
- [30] Blackman M L, Royzen M and Fox J M 2008 Tetrazine Ligation: Fast Bioconjugation Based on Inverse-Electron-Demand Diels-Alder Reactivity *J. Am. Chem. Soc.* **130** 13518-19

-
- [31] Devaraj N K, Weissleder R and Hilderbrand S A 2008 Tetrazine-Based Cycloadditions: Application to Pretargeted Live Cell Imaging *Bioconjugate Chem.* **19** 2297-99
- [32] Cserép G B, Demeter O, Bätzner E, Kállay M, Wagenknecht H-A and Kele P 2015 Synthesis and Evaluation of Nicotinic Acid Derived Tetrazines for Bioorthogonal Labeling *Synthesis* doi: 10.1055/s-0034-1380721
- [33] Karver M R, Weissleder R and Hilderbrand S A 2012 Bioorthogonal Reaction Pairs Enable Simultaneous, Selective, Multi-Target Imaging *Angew. Chem. Int. Ed.* **51** 920-22
- [34] Nikić I, Plass T, Schraidt O, Szymański J, Briggs J A G, Schultz C and Lemke E A 2014 Minimal tags for rapid dual-color live-cell labeling and super-resolution microscopy *Angew. Chem. Int. Ed. Engl.* **53** 2245-9
- [35] Beatty K E 2011 Chemical strategies for tagging and imaging the proteome *Mol. Biosyst.* **7** 2360-67
- [36] Yi L, Sun H, Wu Y-W, Triola G, Waldmann H and Goody R S 2010 A highly efficient strategy for modification of proteins at the C terminus *Angew. Chem. Int. Ed. Engl.* **49** 9417-21
- [37] Gilmore J M, Scheck R A, Esser-Kahn A P, Joshi N S and Francis M B 2006 N-terminal protein modification through a biomimetic transamination reaction *Angew. Chem. Int. Ed. Engl.* **45** 5307-11
- [38] Dixon H B F 1964 Transamination of peptides *Biochem. J.* **92** 661-6
- [39] Stephanopoulos N and Francis M B 2011 Choosing an effective protein bioconjugation strategy *Nat. Chem. Biol.* **7** 876-84
- [40] Morales-Sanfrutos J, Lopez-Jaramillo J, Ortega-Muñoz M, Megia-Fernandez A, Perez-Balderas F, Hernandez-Mateo F and Santoyo-Gonzalez F 2010 Vinyl sulfone: a versatile function for simple bioconjugation and immobilization *Org. Biomol. Chem.* **8** 667-75
- [41] Cserép G B, Baranyai Zs, Komáromy D, Horváti K, Bősze Sz and Kele P 2014 Fluorogenic tagging of peptides via Cys residues using thiol-specific vinyl sulfone affinity tags *Tetrahedron* **70** 5961-65
- [42] Tilley S D and Francis M B 2006 Tyrosine-selective protein alkylation using pi-allylpalladium complexes *J. Am. Chem. Soc.* **128** 1080-1
- [43] Cserép G B, Herner A, Wolfbeis O S and Kele P 2013 Tyrosine specific sequential labeling of proteins *Bioorg. Med. Chem. Lett.* **23** 5776-8
- [44] Zhang G, Zheng S, Liu H and Chen P R 2015 Illuminating biological processes through site-specific protein labeling *Chem. Soc. Rev.* **44** 3405-17
- [45] Rashidian M, Kumarapperuma S C, Gabrielse K, Fegan A, Wagner C R and Distefano M D 2013 Simultaneous dual protein labeling using a triorthogonal reagent. *J. Am. Chem. Soc.* **135** 16388-96
- [46] Los G V, Encell L P, McDougall M G, Hartzell D D, Karassina N, Zimprich C, Wood M G, Learish R, Ohana R F, Urh M, Simpson D, Mendez J, Zimmerman K, Otto P, Vidugiris G, Zhu J, Darzins A, Klaubert D H, Bulleit R F and Wood K V 2008 HaloTag: a novel protein labeling technology for cell imaging and protein analysis. *ACS Chem. Biol.* **3** 373-82
- [47] Lang K and Chin J W 2014 Cellular incorporation of unnatural amino acids and bioorthogonal labeling of proteins *Chem. Rev.* **114** 4764-806
- [48] Grammel M and Hang H C 2013 Chemical reporters for biological discovery *Nat. Chem. Biol.* **9** 475-84
- [49] Ngo J T and Tirrell D A 2011 Noncanonical amino acids in the interrogation of cellular protein synthesis *Acc. Chem. Res.* **44** 677-85

-
- [50] Laughlin S T, Baskin J M, Amacher S L and Bertozzi C R 2008 *In vivo* imaging of membrane-associated glycans in developing zebrafish *Science* **320** 664-7
- [51] Hang H C, Wilson J P and Charron G 2011 Bioorthogonal chemical reporters for analyzing protein lipidation and lipid trafficking *Acc. Chem. Res.* **44** 699-708
- [52] Kostiuk M A, Corvi M M, Keller B O, Plummer G, Prescher J A, Hangauer M J, Bertozzi C R, Rajaiah G, Falck J R and Berthiaume L G 2008 Identification of palmitoylated mitochondrial proteins using a bio-orthogonal azido-palmitate analogue *FASEB J.* **22** 721-32
- [53] Dean K M and Palmer A E 2014 Advances in fluorescence labeling strategies for dynamic cellular imaging *Nat. Chem. Biol.* **10** 512-23
- [54] Wolfbeis O S 2015 An overview of nanoparticles commonly used in fluorescent bioimaging *Chem. Soc. Rev.* doi: 10.1039/c4cs00392f
- [55] Speers A E, Adam G C and Cravatt B F 2003 Activity-Based Protein Profiling in Vivo Using a Copper(I)-Catalyzed Azide-Alkyne [3 + 2] Cycloaddition *J. Am. Chem. Soc.* **125** 4686-7
- [56] Speers A E and Cravatt B F 2004 Profiling Enzyme Activities *In Vivo* Using Click Chemistry Methods *Chem. Biol.* **11** 535-46
- [57] Wright A T and Cravatt B F 2007 Chemical Proteomic Probes for Profiling Cytochrome P450 Activities and Drug Interactions *In Vivo Chem. Biol.* **14** 1043-1051
- [58] Seo T S, Li Z, Ruparel H and Ju J 2003 Click Chemistry to Construct Fluorescent Oligonucleotides for DNA Sequencing *J. Org. Chem.* **68** 609-12
- [59] Li X, Fang T and Boons G-J 2014 Preparation of Well-Defined Antibody–Drug Conjugates through Glycan Remodeling and Strain-Promoted Azide–Alkyne Cycloadditions *Angew. Chem.* **126** 7307-10
- [60] Shao F, Weissleder R and Hilderbrand S A 2008 Monofunctional carbocyanine dyes for bio- and bioorthogonal conjugation *Bioconjugate Chem.* **19** 2487-91
- [61] Sawa M, Hsu T-L, Itoh T, Sugiyama M, Hanson S R, Vogt P K and Wong C-H 2006 Glycoproteomic probes for fluorescent imaging of fucosylated glycans *in vivo Proc. Natl. Acad. Sci. U.S.A.* **103** 12371-6
- [62] Tsou L K, Zhang M M and Hang H C 2009 Clickable fluorescent dyes for multimodal bioorthogonal imaging *Org. Biomol. Chem.* **7** 5055-8
- [63] Lukinavičius G, Umezawa K, Olivier N, Honigsmann A, Yang G, Plass T, Mueller V, Reymond L, Corrêa I R Jr, Luo Z-G, Schultz C, Lemke E A, Heppenstall P, Eggeling C, Manley S and Johnsson K 2013 A near-infrared fluorophore for live-cell super-resolution microscopy of cellular proteins *Nat. Chem.* **5** 132-9
- [64] Yang K S, Budin G, Reiner T, Vinegoni C and Weissleder R 2012 Bioorthogonal Imaging of Aurora Kinase A in Live Cells *Angew. Chem. Int. Ed.* **51** 6598-6603
- [65] Fischer G M, Jüngst C, Isomäki-Kron Dahl M, Gauss D, Möller H M, Daltrozzi E and Zumbusch A 2010 Asymmetric PPCys: Strongly fluorescing NIR labels *Chem. Commun.* **46** 5289-91
- [66] Zhou M, Zhang X, Bai M, Shen D, Xu B, Kao J, Ge X and Achilefu S 2013 Click reaction-mediated functionalization of near-infrared pyrrolopyrrole cyanine dyes for biological imaging applications *RSC Adv.* **3** 6756-8
- [67] Nagy K, Orbán E, Bősze Sz and Kele P 2010 Clickable Long-Wave “Mega-Stokes” Fluorophores for Orthogonal Chemoselective Labeling of Cells *Chem. Asian. J.* **5** 773-7
- [68] Cserép G B, Enyedi K N, Demeter A, Mező G and Kele P 2013 NIR Mega-Stokes Fluorophores for Bioorthogonal Labeling and Energy Transfer Systems—An Efficient Quencher for Daunomycin *Chem. Asian. J.* **8** 494-502

-
- [69] Stubinitzky C, Cserép G B, Bätzner E, Kele P and Wagenknecht H-A 2014 2'-Deoxyuridine conjugated with a reactive monobenzocyclooctyne as a DNA building block for copper-free click-type postsynthetic modification of DNA *Chem. Commun.* **50** 11218-21
- [70] Kiick K L, Saxon E, Tirrell D A and Bertozzi C R 2002 Incorporation of azides into recombinant proteins for chemoselective modification by the Staudinger ligation *Proc. Natl. Acad. Sci. U.S.A.* **99** 19-24
- [71] Wang Q, Chan T R, Hilgraf R, Fokin V V, Sharpless K B and Finn M G 2003 Bioconjugation by Copper(I)-Catalyzed Azide-Alkyne [3 + 2] Cycloaddition *J. Am. Chem. Soc.* **125** 3192-3
- [72] Sivakumar K, Xie F, Cash B M, Long S, Barnhill H N and Wang Q 2004 A Fluorogenic 1,3-Dipolar Cycloaddition Reaction of 3-Azidocoumarins and Acetylenes *Org. Lett.* **6** 4603-6
- [73] Herner A, Nikić I, Kállay M, Lemke E A and Kele P 2013 A new family of bioorthogonally applicable fluorogenic labels *Org. Biomol. Chem.* **11** 3297-306
- [74] Urano Y, Kamiya M, Kanda K, Ueno T, Hirose K and Nagano T 2005 Evolution of Fluorescein as a Platform for Finely Tunable Fluorescence Probes *J. Am. Chem. Soc.* **127** 4888-94
- [75] Goonewardena S N, Leroueil P R, Gemborys C, Tahiliani P, Emery S, Baker J R Jr., Zong H 2013 Fluorogenic 'click-on' dendrimer reporter for rapid profiling of cell proliferation *Bioorg. Med. Chem. Lett.* **23** 2230-3
- [76] Dirksen A, Madsen M, Iacono G D, Matin M J, Bacica M, Stanković N, Callans S and Bhat A 2014 Parallel Synthesis and Screening of Peptide Conjugates *Bioconjugate Chem.* **25** 1052-60
- [77] Xie F, Sivakumar K, Zeng Q, Bruckman M A, Hodges B and Wang Q 2008 A fluorogenic 'click' reaction of azidoanthracene derivatives *Tetrahedron* **64** 2906-14
- [78] Seela F and Pujari S S 2010 Azide-Alkyne "Click" Conjugation of 8-Aza-7-deazaadenine-DNA: Synthesis, Duplex Stability, and Fluorogenic Dye Labeling *Bioconjugate Chem.* **21** 1629-41
- [79] Pujari S S, Ingale S A and Seela F 2014 High-Density Functionalization and Cross-Linking of DNA: "Click" and "Bis-Click" Cycloadditions Performed on Alkynylated Oligonucleotides with Fluorogenic Anthracene Azides *Bioconjugate Chem.* **25** 1855-70
- [80] Koide Y, Urano Y, Hanaoka K, Terai T and Nagano T 2011 Evolution of Group 14 Rhodamines as Platforms for Near-Infrared Fluorescence Probes Utilizing Photoinduced Electron Transfer *ACS Chem. Biol.* **6** 600-8
- [81] Shieh P, Hangauer M J and Bertozzi C R 2012 Fluorogenic Azidofluoresceins for Biological Imaging *J. Am. Chem. Soc.* **134** 17428-31
- [82] Shieh P, Siegrist M S, Cullen A J and Bertozzi C R 2014 Imaging bacterial peptidoglycan with near-infrared fluorogenic azide probes *Proc. Natl. Acad. Sci. U.S.A.* **111** 5456-61
- [83] Shieh P, Dien V T, Beahm B J, Castellano J M, Wyss-Coray T and Bertozzi C R 2015 CalFluors: A universal motif for fluorogenic azide probes across the visible spectrum *J. Am. Chem. Soc.* **137** 7145-51
- [84] Staros J V, Bayley H, Standring D N and Knowles J R 1978 Reduction of Aryl Azides by Thiols: Implications for the Use of Photoaffinity Reagents *Biochem. Biophys. Res. Co.* **80** 568-72
- [85] Shie J-J, Liu Y-C, Lee Y-M, Lim C, Fang J-M and Wong C-H 2014 An Azido-BODIPY Probe for Glycosylation: Initiation of Strong Fluorescence upon Triazole Formation *J. Am. Chem. Soc.* **136** 9953-61

-
- [86] Wang C, Xie F, Suthiwangcharoen N, Sun J and Wang Q 2012 Tuning the optical properties of BODIPY dye through Cu(I) catalyzed azide-alkyne cycloaddition (CuAAC) reaction *Sci. China* **55** 125-30
- [87] Chauhan D P, Saha T, Lahiri M, Talukdar P 2014 BODIPY based 'click on' fluorogenic dyes: application in live cell imaging *Tetrahedron Lett.* **55** 244-7
- [88] Kamaruddin M A, Ung P, Hossain M I, Jarasrassamee B, O'Malley W, Thompson P, Scanlon D, Cheng H-C, Graham B 2011 A facile, click chemistry-based approach to assembling fluorescent chemosensors for protein tyrosine kinases *Bioorg. Med. Chem. Lett.* **21** 329-31
- [89] Hörner A, Volz D, Hagendorn T, Fűrnis D, Greb L, Rönice F, Nieger M, Schepers U and Bräse S 2014 Switchable fluorescence by click reaction of a novel azidocarbazole dye *RSC Adv.* **4** 11528-34
- [90] Herner A, Girona G E, Nikić I, Kállay M, Lemke E A and Kele P 2014 New Generation of Bioorthogonally Applicable Fluorogenic Dyes with Visible Excitations and Large Stokes Shifts *Bioconjugate Chem.* **25** 1370-4
- [91] Zhou Z and Fahrni C J 2004 A Fluorogenic Probe for the Copper(I)-Catalyzed Azide-Alkyne Ligation Reaction: Modulation of the Fluorescence Emission via $^3(n,\pi^*)\text{-}^1(\pi,\pi^*)$ Inversion *J. Am. Chem. Soc.* **126** 8862-3
- [92] Jewett J C and Bertozzi C R 2011 Synthesis of a Fluorogenic Cyclooctyne Activated by Cu-Free Click Chemistry *Org. Lett.* **13** 5937-9
- [93] Friscourt F, Fahrni C J and Boons G-J 2012 A Fluorogenic Probe for the Catalyst-Free Detection of Azide-Tagged Molecules *J. Am. Chem. Soc.* **134** 18809-15
- [94] Lemieux G A, de Graffenried C L and Bertozzi C R 2003 A Fluorogenic Dye Activated by the Staudinger Ligation *J. Am. Chem. Soc.* **125** 4708-9
- [95] Azoulay M, Tuffin G, Sallem W and Florent J-C 2006 A new drug-release method using the Staudinger ligation *Bioorg. Med. Chem. Lett.* **16** 3147-9
- [96] Tsao M-L, Tian F and Schultz P G 2005 Selective Staudinger Modification of Proteins Containing *p*-Azidophenylalanine *ChemBioChem* **6** 2147-9
- [97] Saxon E, Armstrong J I and Bertozzi C R 2000 A "Traceless" Staudinger Ligation for the Chemoselective Synthesis of Amide Bonds *Org. Lett.* **2** 2141-3
- [98] Hangauer M J and Bertozzi C R 2008 A FRET-Based Fluorogenic Phosphine for Live-Cell Imaging with the Staudinger Ligation *Angew. Chem. Int. Ed.* **47** 2394-7
- [99] Cohen A S, Dubikovskaya E A, Rush J S and Bertozzi C R 2010 Real-Time Bioluminescence Imaging of Glycans on Live Cells *J. Am. Chem. Soc.* **132** 8563-5
- [100] Furukawa K, Abe H, Hibino K, Sako Y, Tsuneda S and Ito Y 2009 Reduction-Triggered Fluorescent Amplification Probe for the Detection of Endogenous RNAs in Living Human Cells *Bioconjugate Chem.* **20** 1026-36
- [101] Pianowski Z, Gorska K, Oswald L, Merten C A and Winssinger N 2009 Imaging of mRNA in Live Cells Using Nucleic Acid-Templated Reduction of Azidorhodamine Probes *J. Am. Chem. Soc.* **131** 6492-7
- [102] Clovis J S, Eckell A, Huisgen R and Sustmann R 1967 Der Nachweis des freien Diphenylnitrilimins als Zwischenstufe bei Cycloadditionen *Chem. Ber.* **100** 60-70
- [103] An P, Yu Z and Lin Q 2013 Design of oligothiophene-based tetrazoles for laser-triggered photoclick chemistry in living cells *Chem. Commun.* **49** 9920-2
- [104] Yu Z, Pan Y, Wang Z, Wang J and Lin Q 2012 Genetically Encoded Cyclopropene Directs Rapid, Photoclick-Chemistry-Mediated Protein Labeling in Mammalian Cells *Angew. Chem. Int. Ed.* **51** 10600-4
- [105] Yu Z, Ho L Y and Lin Q 2011 Rapid, Photoactivatable Turn-On Fluorescent Probes Based on an Intramolecular Photoclick Reaction *J. Am. Chem. Soc.* **133** 11912-5

-
- [106] Devaraj N K, Hilderbrand S, Upadhyay R, Mazitschek R and Weissleder R 2010 Bioorthogonal Turn-On Probes for Imaging Small Molecules inside Living Cells *Angew. Chem. Int. Ed.* **49** 2869-72
- [107] Pyka A M, Domnick C, Braun F and Kath-Schorr S 2014 Diels–Alder Cycloadditions on Synthetic RNA in Mammalian Cells *Bioconjugate Chem.* **25** 1438-43
- [108] Asare-Okai P N, Agustin E, Fabris D and Royzen M 2014 Site-specific fluorescence labelling of RNA using bio-orthogonal reaction of trans-cyclooctene and tetrazine *Chem. Commun.* **50** 7844-7
- [109] Holstein J M, Stummer D and Rentmeister A 2015 Enzymatic modification of 5'-capped RNA with a 4-vinylbenzyl group provides a platform for photoclick and inverse electron-demand Diels–Alder reaction *Chem. Sci.* **6** 1362-9
- [110] Lang K, Davis L, Wallace S, Mahesh M, Cox D J, Blackman M L, Fox J M and Chin J W 2012 Genetic Encoding of Bicyclononynes and trans-Cyclooctenes for Site-Specific Protein Labeling *in Vitro* and in Live Mammalian Cells via Rapid Fluorogenic Diels–Alder Reactions *J. Am. Chem. Soc.* **134** 10317-20
- [111] Lang K, Davis L, Torres-Kolbus J, Chou C, Deiters A and Chin J W 2012 Genetically encoded norbornene directs site-specific cellular protein labelling *via* a rapid bioorthogonal reaction *Nat. Chem.* **4** 298-304
- [112] Liu D S, Tangpeerachaikul A, Selvaraj R, Taylor M T, Fox J M and Ting A Y 2012 Diels–Alder Cycloaddition for Fluorophore Targeting to Specific Proteins inside Living Cells *J. Am. Chem. Soc.* **134** 792-5
- [113] Yang J, Šečkutė J, Cole C M and Devaraj N K 2012 Live-Cell Imaging of Cyclopropene Tags with Fluorogenic Tetrazine Cycloadditions *Angew. Chem. Int. Ed.* **51** 7476-9
- [114] Jiao G-S, Thoresen L H and Burgess K 2003 Fluorescent, Through-Bond Energy Transfer Cassettes for Labeling Multiple Biological Molecules in One Experiment *J. Am. Chem. Soc.* **125** 14668-9
- [115] Wan C-W, Burghart A, Chen J, Bergström F, Johansson L B-Å, Wolford M F, Kim T G, Topp M R, Hochstrasser R M and Burgess K 2003 Anthracene-BODIPY Cassettes: Syntheses and Energy Transfer *Chem. Eur. J.* **9** 4430-41
- [116] Carlson J C T, Meimetis L G, Hilderbrand S A and Weissleder R 2013 BODIPY–Tetrazine Derivatives as Superbright Bioorthogonal Turn-on Probes *Angew. Chem. Int. Ed.* **52** 6917-20
- [117] Wiczorek A, Buckup T and Wombacher R 2014 Rigid tetrazine fluorophore conjugates with fluorogenic properties in the inverse electron demand Diels–Alder reaction *Org. Biomol. Chem.* **12** 4177-85
- [118] Wu H, Cisneros B T, Cole C M and Devaraj N K 2014 Bioorthogonal Tetrazine-Mediated Transfer Reactions Facilitate Reaction Turnover in Nucleic Acid-Templated Detection of MicroRNA *J. Am. Chem. Soc.* **136** 17942-5
- [119] Wu H, Yang J, Šečkutė J and Devaraj N K 2014 In Situ Synthesis of Alkenyl Tetrazines for Highly Fluorogenic Bioorthogonal Live-Cell Imaging Probes *Angew. Chem. Int. Ed.* **53** 5805-9
- [120] Meimetis L G, Carlson J C T, Giedt R J, Kohler R H and Weissleder R 2014 Ultrafluorogenic Coumarin–Tetrazine Probes for Real-Time Biological Imaging *Angew. Chem. Int. Ed.* **53** 7531-4
- [121] Madani F, Lind J, Damberg P, Adams S R, Tsien R Y and Gräslund A O 2009 Hairpin Structure of a Biarsenical–Tetracysteine Motif Determined by NMR Spectroscopy *J. Am. Chem. Soc.* **131** 4613-5
- [122] Griffin B A, Adams S R, Tsien R Y 1998 Specific Covalent Labeling of Recombinant Protein Molecules Inside Live Cells *Science* **281** 269-72

-
- [123] Adams S R, Campbell R E, Gross L A, Martin B R, Walkup G K, Yao Y, Llopis J and Tsien R Y 2002 New Biarsenical Ligands and Tetracysteine Motifs for Protein Labeling in Vitro and in Vivo: Synthesis and Biological Applications *J. Am. Chem. Soc.* **124** 6063-76
- [124] Hoffmann C, Gaietta G, Zürn A, Adams S R, Terrillon S, Ellisman M H, Tsien R Y and Lohse M J 2010 Fluorescent labeling of tetracysteine-tagged proteins in intact cells *Nat. Protoc.* **5** 1666-77
- [125] Cao H, Xiong Y, Wang T, Chen B, Squier T C and Mayer M U 2007 A Red Cy3-Based Biarsenical Fluorescent Probe Targeted to a Complementary Binding Peptide *J. Am. Chem. Soc.* **129** 8672-3
- [126] Fu N, Xiong Y, and Squier T C 2012 Synthesis of a Targeted Biarsenical Cy3-Cy5 Affinity Probe for Super-resolution Fluorescence Imaging *J. Am. Chem. Soc.* **134** 18530-3
- [127] Alexander S C and Schepartz A 2014 Interactions of AsCy3 with Cysteine-Rich Peptides *Org. Lett.* **16** 3824-7
- [128] Halo T L, Appelbaum J, Hobert E M, Balkin D M, and Schepartz A 2009 Selective Recognition of Protein Tetraserine Motifs with a Cell-Permeable, Pro-fluorescent Bisboronic Acid *J. Am. Chem. Soc.* **131** 438-9
- [129] Girouard S, Houle M-H, Grandbois A, Keillor J W and Michnick S W 2005 Synthesis and Characterization of Dimaleimide Fluorogens Designed for Specific Labeling of Proteins *J. Am. Chem. Soc.* **127** 559-66
- [130] Guy J, Caron K, Dufresne S, Michnick S W, Skene W G and Keillor J W 2007 Convergent Preparation and Photophysical Characterization of Dimaleimide Dansyl Fluorogens: Elucidation of the Maleimide Fluorescence Quenching Mechanism *J. Am. Chem. Soc.* **129** 11969-77
- [131] Chen Y, Clouthier C M, Tsao K, Strmiskova M, Lachance H and Keillor J W 2014 Coumarin-Based Fluorogenic Probes for No-Wash Protein Labeling *Angew. Chem. Int. Ed.* **53** 13785-8
- [132] Feldborg L N, Jølck R I and Andresen T L 2012 Quantitative evaluation of bioorthogonal chemistries for surface functionalization of nanoparticles *Bioconjugate Chem.* **23** 2444-50
- [133] Murray C B, Norris D J and Bawendi M G 1993 Synthesis and characterization of nearly monodisperse CdE (E = sulfur, selenium, tellurium) semiconductor nanocrystallites *J. Am. Chem. Soc.* **115** 8706-15
- [134] Medintz I L, Uyeda H T, Goldman E R and Mattoussi H 2005 Quantum dot bioconjugates for imaging, labelling and sensing *Nat Mater* **4** 435-46
- [135] Bernardin A, Cazet A, Guyon L, Delannoy P, Vinet F, Bonnaffé D and Texier I 2010 Copper-free click chemistry for highly luminescent quantum dot conjugates: application to in vivo metabolic imaging *Bioconjug. Chem.* **21** 583-8
- [136] Han H-S, Devaraj N K, Lee J, Hilderbrand S A, Weissleder R and Bawendi M G 2010 Development of a bioorthogonal and highly efficient conjugation method for quantum dots using tetrazine-norbornene cycloaddition *J. Am. Chem. Soc.* **132** 7838-9
- [137] Han H-S, Niemeyer E, Huang Y, Kamoun W S, Martin J D, Bhaumik J, Chen Y, Roberge S, Cui J, Martin M R, Fukumura D, Jain R K, Bawendi M G and Duda D G 2015 Quantum dot/antibody conjugates for in vivo cytometric imaging in mice *Proc. Natl. Acad. Sci. U.S.A.* **112** 1350-5
- [138] Pan H, Zhang P, Gao D, Zhang Y, Li P, Liu L, Wang C, Wang H, Ma Y and Cai L 2014 Noninvasive visualization of respiratory viral infection using bioorthogonal conjugated near-infrared-emitting quantum dots *ACS Nano* **8** 5468-77

-
- [139] Auzel F 2004 Upconversion and anti-Stokes processes with f and d ions in solids *Chem. Rev.* **104** 139-74
- [140] Wang F and Liu X 2009 Recent advances in the chemistry of lanthanide-doped upconversion nanocrystals *Chem. Soc. Rev.* **38** 976-89
- [141] Mader H S, Kele P, Saleh S M and Wolfbeis O S 2010 Upconverting luminescent nanoparticles for use in bioconjugation and bioimaging *Curr. Opin. Chem. Biol.* **14** 582-96
- [142] Mader H S, Link M, Achatz D E, Uhlmann K, Li X and Wolfbeis O S 2010 Surface-Modified Upconverting Microparticles and Nanoparticles for Use in Click Chemistries *Chem. Eur. J.* **16** 5416-24
- [143] Rubner M M, Achatz D E, Mader H S, Stolwijk J A, Wegener J, Harms G S, Wolfbeis O S and Wagenknecht H-A 2012 DNA "Nanolamps": "Clicked" DNA Conjugates with Photon Upconverting Nanoparticles as Highly Emissive Biomaterial *ChemPlusChem* **77** 129-34
- [144] Boyer J-C, Carling C-J, Chua S Y, Wilson D, Johnsen B, Baillie D and Branda N R 2012 Photomodulation of Fluorescent Upconverting Nanoparticle Markers in Live Organisms by Using Molecular Switches *Chem. Eur. J.* **18** 3122-6
- [145] Beyazit S, Ambrosini S, Marchyk N, Palo E, Kale V, Soukka T, Tse Sum Bui B and Haupt K 2014 Versatile Synthetic Strategy for Coating Upconverting Nanoparticles with Polymer Shells through Localized Photopolymerization by Using the Particles as Internal Light Sources *Angew. Chem. Int. Ed.* **53** 8919-23
- [146] Faklaris O, Joshi V, Irinopoulou T, Tauc P, Sennour M, Girard H, Gesset C, Arnault J-C, Thorel A, Boudou J-P, Curmi P A and Treussart F 2009 Photoluminescent Diamond Nanoparticles for Cell Labeling: Study of the Uptake Mechanism in Mammalian Cells *ACS Nano* **3** 3955-62
- [147] Schrand A M, Huang H, Carlson C, Schlager J J, Ōsawa E, Hussain S M and Dai L 2007 Are diamond nanoparticles cytotoxic? *J. Phys. Chem. B* **111** 2-7
- [148] Rehor I, Slegerova J, Kucka J, Proks V, Petrakova V, Adam M-P, Treussart F, Turner S, Bals S, Sacha P, Ledvina M, Wen A M, Steinmetz N F and Cigler P 2014 Fluorescent Nanodiamonds Embedded in Biocompatible Translucent Shells *Small* **10** 1106-15
- [149] Rehor I, Mackova H, Filippov S K, Kucka J, Proks V, Slegerova J, Turner S, van Tendeloo G, Ledvina M, Hruby M and Cigler P 2014 Fluorescent Nanodiamonds with Bioorthogonally Reactive Protein-Resistant Polymeric Coatings *ChemPlusChem* **79** 21-4
- [150] Mader H, Li X, Saleh S, Link M, Kele P, and Wolfbeis O S 2008 Fluorescent silica nanoparticles *Ann. N. Y. Acad. Sci.* **1130** 218-23
- [151] Lai C-H, Chang T-C, Chuang Y-J, Tzou D-L and Lin C-C 2013 Stepwise orthogonal click chemistry toward fabrication of paclitaxel/galactose functionalized fluorescent nanoparticles for HepG2 cell targeting and delivery *Bioconjugate Chem.* **24** 1698-709
- [152] Kele P, Mező G, Achatz D and Wolfbeis O S 2009 Dual labeling of biomolecules by using click chemistry: a sequential approach *Angew. Chem. Int. Ed.* **48** 344-7
- [153] Achatz D E, Mező G, Kele P and Wolfbeis O S 2009 Probing the activity of matrix metalloproteinase II with a sequentially click-labeled silica nanoparticle FRET probe *ChemBioChem* **10** 2316-20
- [154] Haun J B, Devaraj N K, Hilderbrand S A, Lee H and Weissleder R 2010 Bioorthogonal chemistry amplifies nanoparticle binding and enhances the sensitivity of cell detection *Nat. Nanotechnol.* **5** 660-5
- [155] Chung H J, Castro C M, Im H, Lee H and Weissleder R 2013 A magneto-DNA nanoparticle system for rapid detection and phenotyping of bacteria *Nat. Nanotechnol.* **8** 369-75

-
- [156] Haun J B, Devaraj N K, Marinelli B S, Lee H and Weissleder R 2011 Probing intracellular biomarkers and mediators of cell activation using nanosensors and bioorthogonal chemistry *ACS Nano* **5** 3204-13
- [157] Wu C, Szymanski C, Cain Z and McNeill J 2007 Conjugated polymer dots for multiphoton fluorescence imaging *J. Am. Chem. Soc.* **129** 12904-5
- [158] Wu C, Bull B, Szymanski C, Christensen K and McNeill J 2008 Multicolor conjugated polymer dots for biological fluorescence imaging *ACS Nano* **2** 2415-23
- [159] Moon J H, McDaniel W, MacLean P and Hancock L F 2007 Live-Cell-Permeable Poly(p-phenylene ethynylene) *Angew. Chem. Int. Ed.* **46** 8223-25
- [160] Wu C, Jin Y, Schneider T, Burnham D R, Smith P B and Chiu D T 2010 Ultrabright and Bioorthogonal Labeling of Cellular Targets Using Semiconducting Polymer Dots and Click Chemistry *Angew. Chem. Int. Ed.* **49** 9436-40
- [161] Petersen A L, Hansen A E, Gabizon A and Andresen T L 2012 Liposome imaging agents in personalized medicine *Adv. Drug Deliv. Rev.* **64** 1417-35
- [162] Phillips M A, Gran M L and Peppas N A 2010 Targeted nanodelivery of drugs and diagnostics *Nano Today* **5** 143-59
- [163] Maeda H, Wu J, Sawa T, Matsumura Y and Hori K 2000 Tumor vascular permeability and the EPR effect in macromolecular therapeutics: a review *J. Control Release* **65** 271-84
- [164] Koo H, Lee S, Na J H, Kim S H, Hahn S K, Choi K, Kwon I C, Jeong S Y and Kim K 2012 Bioorthogonal copper-free click chemistry in vivo for tumor-targeted delivery of nanoparticles *Angew. Chem. Int. Ed.* **51** 11836-40